

**BULETINUL
INSTITUTULUI
POLITEHNIC
DIN IAȘI**

**Volumul 63 (67)
Numărul 4**

**Secția
MATEMATICĂ
MECANICĂ TEORETICĂ
FIZICĂ**

2017

Editura POLITEHNIUM

BULETINUL INSTITUTULUI POLITEHNIC DIN IAȘI
PUBLISHED BY
“GHEORGHE ASACHI” TECHNICAL UNIVERSITY OF IAȘI
Editorial Office: Bd. D. Mangeron 63, 700050, Iași, ROMANIA
Tel. 40-232-278683; Fax: 40-232-237666; e-mail: polytech@mail.tuiasi.ro

Editorial Board

President: **Dan Cașcaval**,
Rector of the “Gheorghe Asachi” Technical University of Iași
Editor-in-Chief: **Maria Carmen Loghin**,
Vice-Rector of the “Gheorghe Asachi” Technical University of Iași
Honorary Editors of the Bulletin: **Alfred Braier**,
Mihail Voicu, Corresponding Member of the Romanian Academy,
Carmen Teodosiu

Editors in Chief of the **MATHEMATICS. THEORETICAL MECHANICS.**
PHYSICS Section

Maricel Agop, Narcisa Apreutesei-Dumitriu,
Daniel Condurache

Honorary Editors: **Cătălin Gabriel Dumitraș**

Associated Editor: **Petru Edward Nica**

Scientific Board

Sergiu Aizicovici, University “Ohio”, U.S.A.
Constantin Băcuță, University “Delaware”, Newark,
Delaware, U.S.A.

Masud Caichian, University of Helsinki, Finland

Adrian Cordunenu, “Gheorghe Asachi” Technical
University of Iași

Constantin Corduneanu, University of Texas,
Arlington, USA.

Piergiulio Corsini, University of Udine, Italy

Sever Dragomir, University “Victoria”, of Melbourne,
Australia

Constantin Fetecău, “Gheorghe Asachi” Technical
University of Iași

Cristi Foça, University of Lille, France

Tasawar Hayat, University “Quaid-i-Azam” of
Islamabad, Pakistan

Radu Ibănescu, “Gheorghe Asachi” Technical
University of Iași

Bogdan Kazmierczak, Inst. of Fundamental Research,
Warsaw, Poland

Liviu Leontie, “Al. I. Cuza” University, Iași
Rodica Luca-Tudorache, “Gheorghe Asachi”
Technical University of Iași

Radu Miron, “Al. I. Cuza” University of Iași
Iuliana Oprea, Colorado State University, U.S.A
Viorel-Puiu Păun, University “Politehnica” of
București

Lucia Pletea, “Gheorghe Asachi” Technical
University of Iași

Irina Radinschi, “Gheorghe Asachi” Technical
University of Iași

Themistocles Rassias, University of Athens, Greece

Behzad Djafari Rouhani, University of Texas at El
Paso, USA

Cristina Stan, University “Politehnica” of București
Wenchang Tan, University “Peking” Beijing, China

Petre P. Teodorescu, University of București

Anca Tureanu, University of Helsinki, Finland

Vitaly Volpert, CNRS, University “Claude Bernard”,
Lyon, France

Secția

MATEMATICĂ. MECANICĂ TEORETICĂ. FIZICĂ

S U M A R

	<u>Pag.</u>
MĂDĂLINA ALBU, IUSTINA HĂTESCU, CĂLIN GHEORGHE BUZEA, CAMIL CIPRIAN MIREȘTEAN, CĂTĂLIN BORCIA, ROXANA IRINA IANCU și DRAGOȘ TEODOR IANCU, Evaluarea comparativă a riscului de xerostomie cu ajutorul modelelor radiobiologice pentru pacienții cu neoplasme de nazofaringe și orofaringe local avansate, iradiate prin tehnicile IMRT și VMAT (engl., rez. rom.)	9
TUDOR CIOBANU, ALINA ROGOJANU, IRINA BUTUC, CAMIL CIPRIAN MIREȘTEAN, CĂLIN GHEORGHE BUZEA și DRAGOȘ TEODOR IANCU, Efectul dozimetric asupra structurilor neuronale ale radioterapiei IMRT și VMAT care protejează scalpul în cazul gliomelor de grad înalt (engl., rez. rom.)	19
ALINA ROGOJANU, ALEXANDRU ZARA, CAMIL CIPRIAN MIREȘTEAN, CĂLIN GHEORGHE BUZEA și DRAGOȘ TEODOR IANCU, Efectul escaladării dozei și a dimensiunii volumului țintă asupra riscului de toxicitate rectală tardivă în radioterapia neoplasmelor de prostată local avansate (engl., rez. rom.)	27
RODICA LUCA, Existența soluțiilor pozitive pentru o problemă la limită fracționară (engl., rez. rom.)	37
ȘTEFAN ANDREI IRIMICIUC și BIANCA CRISTIANA HODOROABĂ, Ablajia laser: Stadiu actual și perspective (engl., rez. rom.)	51
IRINEL CASIAN BOTEZ, IULIANA OPREA și MARICEL AGOP, Teoria “embedding” pentru sisteme complexe (engl., rez. rom.)	69

Section

MATHEMATICS. THEORETICAL MECHANICS. PHYSICS

CONTENTS

	<u>Pp.</u>
MĂDĂLINA ALBU, IUSTINA HĂTESCU, CĂLIN GHEORGHE BUZEA, CAMIL CIPRIAN MIREȘTEAN, CĂTĂLIN BORCIA, ROXANA IRINA IANCU and DRAGOȘ TEODOR IANCU, Comparative Evaluation of the Risk of Xerostomia Using Radiobiological Models for Patients with Locally Advanced Nasopharynx and Oropharynx Neoplasm, Irradiated with IMRT and VMAT Techniques (English, Romanian summary)	9
TUDOR CIOBANU, ALINA ROGOJANU, IRINA BUTUC, CAMIL CIPRIAN MIREȘTEAN, CĂLIN GHEORGHE BUZEA and DRAGOȘ TEODOR IANCU, Dosimetric Effect on Neural Structures of Scalp-Sparing IMRT and VMAT Radiotherapy for High-Grade Gliomas (English, Romanian summary)	19
ALINA ROGOJANU, ALEXANDRU ZARA, CAMIL CIPRIAN MIREȘTEAN, CĂLIN GHEORGHE BUZEA and DRAGOȘ TEODOR IANCU, The Effect of Dose Escalation and of the Size of the Target Volume on Late Rectal Toxicity Risk in Advanced Localized Prostate Cancer (English, Romanian summary)	27
RODICA LUCA, Existence of Positive Solutions for a Fractional Boundary Value Problem (English, Romanian summary)	37
ȘTEFAN ANDREI IRIMICIUC and BIANCA CRISTIANA HODOROABĂ, Laser Ablation: State of the Art and Perspectives (English, Romanian summary)	51
IRINEL CASIAN BOTEZ, IULIANA OPREA and MARICEL AGOP, Embedding Theory in Complex Systems (English, Romanian summary)	69

BULETINUL INSTITUTULUI POLITEHNIC DIN IAȘI
Publicat de
Universitatea Tehnică „Gheorghe Asachi” din Iași
Volumul 63 (67), Numărul 4, 2017
Secția
MATEMATICĂ. MECANICĂ TEORETICĂ. FIZICĂ

**COMPARATIVE EVALUATION OF THE RISK OF
XEROSTOMIA USING RADIOBIOLOGICAL MODELS FOR
PATIENTS WITH LOCALLY ADVANCED NASOPHARYNX
AND OROPHARYNX NEOPLASM, IRRADIATED WITH IMRT
AND VMAT TECHNIQUES**

BY

**MĂDĂLINA ALBU¹, IUSTINA HĂTESCU¹, CĂLIN GHEORGHE BUZEA^{2,*},
CAMIL CIPRIAN MIREȘTEAN², CĂTĂLIN BORCIA¹,
ROXANA IRINA IANCU^{3,4} and DRAGOȘ TEODOR IANCU^{2,3}**

¹“Alexandru Ioan Cuza” University of Iași

²Regional Institute of Oncology, Iași

³“Grigore T. Popa” University of Medicine and Pharmacy, Iași

⁴“Sf. Spiridon” Emergency Clinical Hospital, Iași

Received: October 23, 2017

Accepted for publication: December 22, 2017

Abstract. Xerostomia is a frequent cause of damage of the quality of life of a patient treated with radiotherapy for head and neck neoplasm. Prevention is the most recommended attitude because the management of xerostomia is rarely effective. Several strategies have been developed to avoid radiation-induced salivary dysfunction. They imply radiation techniques know to spare salivary glands: intensity modulated radiotherapy (IMRT) and volumetric modulated arc therapy (VMAT). For 20 patients with oro- and nasopharyngeal cancer, treated with IMRT/VMAT, the risk of xerostomia was computed with the radiobiological models Lyman, Kutcher, Burman (LKB) and EUD (Equivalent Uniform Dose)-based. These models' inputs are the dose-volume histograms (DVH) calculated by the treatment planning system (TPS). The values obtained vary from one model to the other, for the same technique and patient.

*Corresponding author; *e-mail*: calinb2003@yahoo.com

Radiobiological models are not implemented as a standard in clinical practice but may provide predictive values for irradiation-related toxicity.

Keywords: xerostomia; radiobiological models; IMRT; VMAT; head and neck neoplasm.

1. Introduction

Xerostomia is one of the most common complications during and after radiotherapy for head and neck cancer, because irreparable damage is caused to the salivary glands included in the radiation fields. Xerostomia can be permanent, leading to severe damage to deglutition function, taste and to oral cavity infections and dental caries because of the altered composition and salivary pH. Parotid glands produce 60% of total saliva, submandibular glands 20% and the rest is produced by sublingual and accessory salivary glands. The acute effects can be reversible if the allowed doses are not overcrossed for the parotid glands. QUANTEC dosimetric recommendations for reducing xerostomia are a mean dose lower than 26Gy for bilateral parotid gland, and lower than 20Gy for unilateral ones. If it is not possible to follow dosimetric constrains, the next step is to reduce dose to only one of the parotids to less than 26Gy, in order to save at least one of two. The clinical benefit of protecting the submandibular glands is controversial. Maintaining them at a mean dose less than 39Gy could preserve their function (Ortholan *et al.*, 2010; Buzalaf *et al.*, 2012; Deasy *et al.*, 2010).

Xerostomia is a frequent cause of damage of the quality of life of a patient treated with radiotherapy for ORL neoplasm. Prevention is one of the most important recommended attitude because the management of xerostomia is rarely effective. Several strategies have been developed to avoid radiation-induced salivary dysfunction without definitively compromising the oncologic treatment. These strategies imply salivary gland-sparing radiation techniques: IMRT (intensity modulated radiotherapy) and VMAT (volumetric modulated arc therapy). For complex dose distribution differing from that provided by the 3D-CRT radiotherapy technique, radiobiological models may have a predictive value superior to univariate assessment for prediction of high grade xerostomia (Abel *et al.*, 2017).

2. Materials and Methods

For 34 patients treated with definitive radiotherapy using IMRT or VMAT techniques for oro- and nasopharynx cancer, the risk of xerostomia was calculated with the help of mathematical models: Lyman Kutcher Burman and EUD-based. They are centered on several parameters such as TD50, n, m, etc. These models come into shape with the help of the dose-volume histogram

(DVH). The values obtained vary from one model to another, for the same technique and patient (Gabryś *et al.*, 2017).

CT scans with a slice thickness of 3 mm were acquired from the aortic arch to the vertex. Weekly during treatment, following the initial setup, an orthogonal pair of kV radiographs were acquired using the Varian On Board Imaging (OBI) system (Varian Medical Systems, Palo Alto, CA), and manually by the therapists using the Varian OBI application and the necessary (manual 2D-2D). The registering of acquired images to the simulation DRRs was made by the radiation therapist to determine setup errors and corrective couch shifts (Kang *et al.*, 2010).

GTV (gross tumor volume) was delineated using image fusion and a rigid registration algorithm. CT (computer tomography) and MRI (magnetic resonance imaging) with contrast agent as well as clinical examination data and endoscopic evaluation were used to delineate the anatomical limits of GTV volume (Fig. 1). Three CTVs (clinical target volumes) with a risk for microscopic dissemination are defined: a high dose CTV70 disease; a high risk CTV66 reflecting the high risk of local spread in and adjacent to the nasopharynx and oropharynx and a prophylactic CTV50 to treat the at risk but uninvolved nodes. A CTV-PTV margin is applied (3–5 mm) based on set-up errors, assuming no tumor motion (Dobbs *et al.*, 2009).

Doses of 70Gy/35 daily fractions in 7 weeks plus concomitant cisplatin or 3-4 cycles of platinum based induction chemotherapy, 66Gy/33 fractions on high risk lymph nodes PTV and 50Gy/25 fractions on low risk lymph nodes levels were administrated in three treatment phases (sequential boost) (Brouwer *et al.*, 2015).

VMAT plans using the Varian RapidArc technique (Varian Medical Systems, Palo Alto, CA) were planned using Eclipse Version 11.0.31 treatment planning software using the same CT-dataset and contoured volumes as the IMRT plans. A single arc technique was used with the gantry set to rotate through 360° in a clockwise direction from a starting position of 181° to a final position of 179°, and a double arc technique with the gantry set to rotate through 360° in a clockwise direction from a starting position of 181° to a final position of 179°, and through 360° in a counterclockwise direction from a starting position of 179° to a final position of 181° according to the complexity of the phase being treated. The collimator rotation was individually optimized for each patient but generally set at 30° and 330° to reduce the effect of tongue and groove leakage (Figs. 2 and 3).

Radiobiological models can be divided into two categories: empiric and theoretical. Empiric models are based on the fitting curves to the actual clinical data. These models are valid only if they are described by initial clinical data. On the other hand, theoretical models are described with the help of radiation interaction with cells and DNA, and also with the help of the processes involved. When using radiobiological models, you have to take into

consideration the fact that they do not have a wide applicability due to the fact that there are no sufficient laboratory data.

Normal tissue complication probability (NTCP) is defined as the percentage of radiotreated patients which develop certain reactions, at a certain dose, at a tissue located near the tumor mass. Manifestation of a specific effect of a normal tissue is also known as clinical endpoint. These endpoints can be divided into two groups. The first one includes functional changes such as paralysis and death, which occur at a narrow dose range. The second one refers to physiological and extensive reactions, and these ones can be developed for a wider dose range, with a direct relation between dose and severity of the reaction.

There are two models that were used to calculate the risk of xerostomia, Lyman-Kutcher Burman and EUD.

The first one, LKB model, is described by the following formula:

$$NTCP = \frac{1}{\sqrt{2\pi}} \int_{-\infty}^t e^{-\frac{x^2}{2}} dx \quad (1)$$

where

$$t = \frac{D_{ef} - TD_{50}}{mTD_{50}} \quad (2)$$

and

$$D_{ef} = (\sum_i v_i D_i^{1/n})^n \quad (3)$$

D_{ef} is the dose that, administrated uniformly to the entire volume will lead to the same NTCP as the real unevenly distributed dose, and D_i is the dose given to the sub volume v_i . The volume dependence of complication probability is given by parameter n , and the complication probability slope comparing to the dose curve is given by m . TD_{50} is the dose given to the entire organ which would lead to a complication probability of 50%.

EUD based model is defined as the equivalent biological dose, which when unevenly distributed, will lead to the same biological effect as the real distribution of the unevenly dose distribution.

$$EUD = (\sum_i v_i D_i^a)^{\frac{1}{a}} \quad (4)$$

D_i is the dose received by a subvolume v_i and a is a parameter that has no dimension and it's specific for every tissue

NTCP can be calculated with the help of formula

$$NTCP = \frac{1}{1 + (\frac{TD_{50}}{EUD})^{4\gamma_{50}}} \quad (5)$$

Where γ_{50} is also a dimensionless parameter, specific for every tissue, describing dose-response curve.

3. Results

NTCP obtained using the EUD radiobiological model provided values between 0 and 26.46% with an average value for the right parotid of 7.38% for IMRT and 3.89% for VMAT. For the left parotid, the average value is 9.08% for IMRT and 3.75% for VMAT. For the LKB model, the NTCP values ranged between 7.23 and 37.49% with an average value for the right parotid of 24.33% for IMRT and 20.74% for VMAT. For the left parotid 25.27% for IMRT and 22.49% for VMAT (complete values in Table 1 and 2, see also the diagram from Fig. 4).

Higher values were obtained using the LKB model than the EUD model.

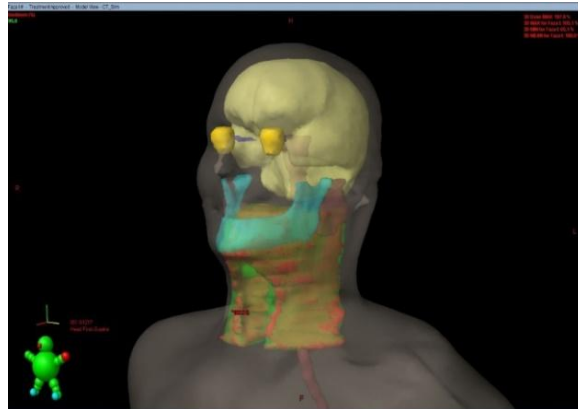


Fig. 1 – Organs at risk and target volume, 3D reconstruction using VARIAN Eclipse TPS.

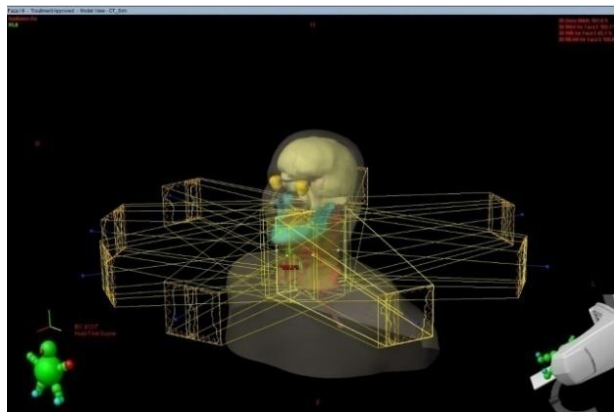


Fig. 2 – IMRT field orientation.

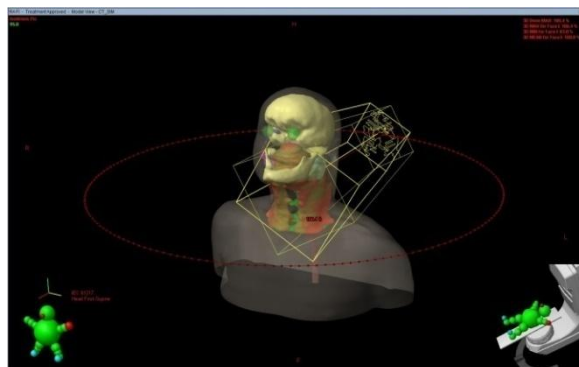


Fig. 3 – VMAT field orientation.

Table 1
NTCP Calculated for Patients Treated with VMAT Techniques

Patient	Left parotid (%)		Right parotid (%)	
	LKB	EUD	LKB	EUD
1	27.97	7.35	29.47	9.43
2	16.49	0.49	14.38	0.19
3	23.77	3.24	25.41	4.84
4	34.03	17.93	32.26	14.22
5	26.64	5.76	23.52	3.05
6	27	6.17	26.77	5.9
7	15.99	0.36	14.96	0.24
8	24.53	3.81	23.35	2.95
9	18.06	0.72	20.63	1.51
10	25.91	5.03	29.03	8.77
11	24.06	3.46	18.3	0.78
12	20.52	1.52	25.31	4.57
13	21.51	1.98	23.32	3.01
14	21.06	1.73	19.36	1.1
15	25	4.2	26.56	5.7
16	27.68	6.99	30.18	10.53
17	27.23	6.45	31.19	12.3

Table 2
NTCP Values Calculated for Patients Treated with IMRT

Patient	Left parotid (%)		Right parotid (%)	
	LKB	EUD	LKB	EUD
1	36.43	23.73	37.49	26.46
2	32.98	15.71	35.28	20.88
3	11.5	0.04	13.6	0.11
4	12.25	0.06	7.23	0
5	28.56	8.1	23.52	3.08
6	36.39	23.65	32.07	13.99
7	33.73	17.49	31.64	13.35
8	26.64	5.78	29.66	9.7
9	17.92	0.72	17.22	0.57
10	21.65	2.04	25.94	5.13
11	22.02	2.21	20.39	1.46
12	25.56	4.7	25.63	4.79
13	32.72	15.19	26.66	5.83
14	20.23	1.38	25.03	4.24
15	36.67	24.43	28.75	8.44
16	9.12	0.01	9.16	0.01

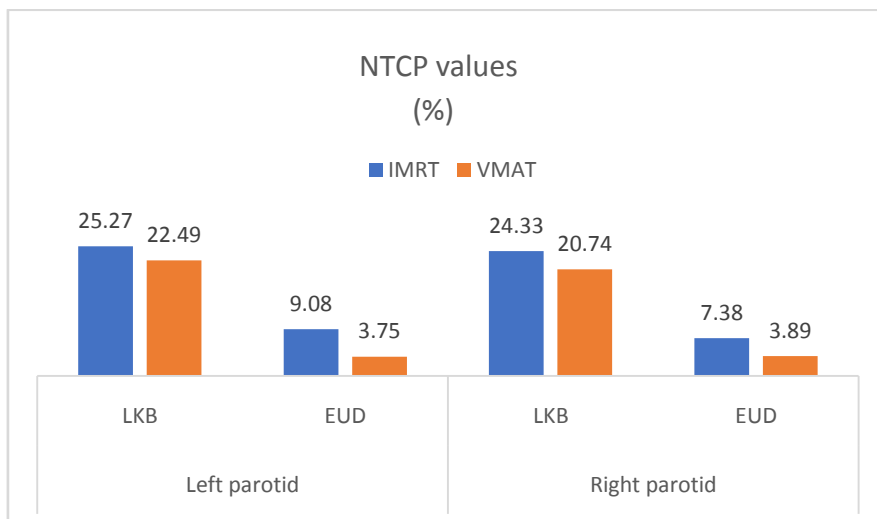


Fig. 4 – Diagram with average values for NTCP.

4. Discussion

White *et al.* demonstrates the equivalence or even superiority of VMAT technique to IMRT technique in target volume coverage and OAR protection with a considerable benefit in reducing the treatment time with possible positive radiobiological consequences. Doses to parotid glands and their NTCPs were significantly lower for VMAT plans (White *et al.*, 2013).

The reduction of the salivary flow rate causes functional impairment and patient discomfort including the inability to articulate, a dry mouth, the inability to chew and swallow food and halitosis with an important impact on the patient's social life. The Common Terminology Criteria for Adverse Effects (CTCAE) was used to describes gradually possible side effects (Grade 2 effects are moderate, Grade 3 effects are considered severe and are associated with possible treatment disruption) (Hanley and Leech, 2016).

Some authors have shown that the LKB model has the advantage of differentiating the risk of severe xerostomia for cases where QUANTEC recommendations are exceeded. Unfortunately, radiobiological models have not shown a predictive value for low or moderate grade xerostomia (Houweling *et al.*, 2010).

In a thirty-two patients cohort with non-metastatic nasopharyngeal cancer curatively treated using VMAT (RapidArc), Layla *et al.* reported a 9.4% grade 3 xerostomia, concluding that the VMAT technique offers a good sparing of organs at risk especially the nervous structures and salivary glands and an excellent target volume coverage (Lalya *et al.*, 2017).

On a radiobiological model trained on the PARSPORT trial data, Gabryś *et al.* considered that the LKB model predicts quite correctly the risk of xerostomia between G1 and G2 grade, from moderate to severe xerostomia, but it does not provide accuracy for cases where the parotid mean dose is in the low-dose domain. The same predictive limit value is also proven if the parotid mean dose exceeds the QUANTEC tolerance recommendations (Gabryś *et al.*, 2017).

5. Conclusions

Radiobiological models are ideal mathematical models, not clinically validated but have orientative value in therapeutic decision and radiotherapy plan optimization. The risk of xerostomia is influenced by different factors such as age, sex, smoker status, chemotherapy treatment, personal medication for comorbidities. Concluding values individually tailored can be reached by multivariate analysis including clinical, biological and dosimetric variables.

Values obtained for the two techniques are similar, proving that VMAT technique is not inferior to IMRT, which is considered to be standard in head & neck radiotherapy.

Higher values of NTCP lead to the necessity of optimizing treatment plans in order to reduce/lower doses to parotids. They have a guiding purpose when DVH curve analysis can not provide an intuitive risk of xerostomia due to complex dose distribution.

REFERENCES

- Abel E., Silander E., Nyman J. *et al.*, *Impact on Quality of Life of IMRT versus 3-D Conformal Radiation Therapy in Head and Neck Cancer Patients: A Case Control Study*, *Adv. Radiat. Oncol.*, May 12, **2**, 3, 346-353 (2017).
- Brouwer C.L., Steenbakkens R.J., Bourhis J. *et al.*, *CT-Based Delineation of Organs at Risk in the Head and Neck Region: DAHANCA, EORTC, GORTEC, HKNPCSG, NCIC CTG, NCRI, NRG Radiother Oncol.*, Oct., **117**, 1, 83-90 (2015).
- Buzalaf M.A.R., Hannas A.R., Kato M.T., *Saliva and Dental Erosion*, *J. Appl. Oral Sci.*, Sep-Oct, **20**, 5, 493-502 (2012).
- Deasy J.O., Moiseenko V., Marks L. *et al.*, *Radiotherapy Dose-Volume Effects on Salivary Gland Function*, *Int. J. Radiat. Oncol. Biol. Phys.*, Mar. 1, **76**, (3 Suppl): S58-63 (2010).
- Dobbs J.E., Barrett A., Roques T., *Practical Radiotherapy Planning*, Fourth Edition, Boca Raton, Florida: CRC Press (2009).
- Gabryś H.S., Buettner F., Sterzing F., *Parotid Gland Mean Dose as a Xerostomia Predictor in Low-Dose Domains*, *Acta Oncol.*, 2017, Sep., **56**, 9, 1197-1203.
- Hanley O., Leech M. *Reduction of Xerostomia in Head and Neck Cancer Patients. A Critical Review of the Literature*, *Radiography*, **22** (2016) S57- S63.
- Houweling A.C., Philippens M.E., Dijkema T. *et al.*, *A Comparison of Dose-Response Models for the Parotid Gland in a Large Group of Head-and-Neck Cancer Patients*, *Int. J. Radiat. Oncol. Biol. Phys.*, 2010, Mar. 15, **76**, 4, 1259-1265.
- Kang H., Lovelock D.M., Yorke E.D., *Accurate Positioning for Head and Neck Cancer Patients Using 2D and 3D Image Guidance*, *J. Appl. Clin. Med. Phys.*, 2010, Oct. 27, **12**, 1, 3270.
- Lalya I., Marnouche E.A., Abdelhak M. *et al.*, *Radiotherapy of Nasopharyngeal Cancer Using Rapidarc: Dosimetric Study of Military Teaching Hospital Mohamed V, Morocco*, *BMC Res Notes*, 2017, Feb. 28, **10**, 1, 112, doi:10.1186/s13104-017-2430-2.
- Ortholan C., Benezy K., Bensadoun R.J. *et al.*, *Normal Tissue Tolerance to External Beam Radiation Therapy: Salivary Glands* (Article in French), *Cancer Radiother.*, 2010, Jul., **14**, 4-5, 290-294.
- White P., Chan K.C., Cheng K.W. *et al.*, *Volumetric Intensity-Modulated Arc Therapy vs. Conventional Intensity-Modulated Radiation Therapy in Nasopharyngeal Carcinoma: A Dosimetric Study*, *J. Radiat. Res.*, 2013, May, **54**, 3, 532-545.

EVALUAREA COMPARATIVĂ A RISCULUI DE XEROSTOMIE CU AJUTORUL
MODELELOR RADIOBIOLOGICE PENTRU PACIENȚII CU NEOPLASME DE
NAZOFARINGE ȘI OROFARINGE LOCAL AVANSATE,
IRADIATE PRIN TEHNICILE IMRT ȘI VMAT

(Rezumat)

Xerostomia este o cauză frecventă a afectării calității vieții unui pacient cu neoplasm al capului și gâtului radiotratat. Prevenția este una dintre cele mai importante atitudini recomandate, deoarece administrarea xerostomiei este rareori eficientă. Au fost dezvoltate mai multe strategii pentru a evita disfuncțiile salivare induse de radiații. Aceste strategii implică tehnici de iradiere care știu să ocolească glandele salivare: IMRT (radioterapia modulată în intensitate) și VMAT (terapie în arc modulată volumetric).

Pentru 20 de pacienți diagnosticați cu cancer oro- și nazofaringian, tratați cu tehnicile IMRT sau VMAT, riscul de xerostomie a fost calculat cu ajutorul modelelor radiobiologice: Lyman Kutcher Burman (LKB) și bazate pe EUD (Doză Uniformă Echivalentă). Datele de intrare ale acestor modele sunt histogramele doză-volum (DVH) calculate de sistemul de planificare a tratamentului (TPS). Valorile obținute variază de la un model la altul, pentru aceeași tehnică și același pacient. De obicei, se obțin valori mai mari utilizând modelul LKB decât modelul EUD. Modelele radiobiologice nu sunt implementate ca standard în practica clinică, dar oferă o valoare predictivă pentru toxicitățile asociate iradierii.

BULETINUL INSTITUTULUI POLITEHNIC DIN IAȘI
Publicat de
Universitatea Tehnică „Gheorghe Asachi” din Iași
Volumul 63 (67), Numărul 4, 2017
Secția
MATEMATICĂ. MECANICĂ TEORETICĂ. FIZICĂ

DOSIMETRIC EFFECT ON NEURAL STRUCTURES OF SCALP-SPARING IMRT AND VMAT RADIOTHERAPY FOR HIGH-GRADE GLIOMAS

BY

TUDOR CIOBANU¹, ALINA ROGOJANU¹, IRINA BUTUC¹,
CAMIL CIPRIAN MIREȘTEAN¹, CĂLIN GHEORGHE BUZEA^{1,*} and
DRAGOȘ TEODOR IANCU^{1,2}

¹Regional Institute of Oncology, Iași

²“Grigore T. Popa” University of Medicine and Pharmacy, Iași

Received: October 23, 2017

Accepted for publication: December 22, 2017

Abstract. Radiotherapy for brain tumors with hair follicle protection for alopecia reduction has become a viable option with the introduction of inverse planning radiotherapy techniques. The aim of the study was the evaluation of the possibility of reducing the maximum and the medium dose received by the scalp for 3 cases of temporoparietal glioblastoma patients irradiated with a total dose of 60Gy and the effect of applying this constraint on other radiosensitive anatomical structures. In all three cases a reduction in mean doses of 5.5%, 3.2% and 12.5% was achieved using the modulated intensive radiotherapy technique (IMRT) and 5.1%, 0.8% and 22.2% by volumetric modulated arc therapy (VMAT) and a reduction of maximum dose by 18.7%, 9.6% and 8.3% using IMRT technique and by 16.35%, 11% and 16% using VMAT technique with no increase in dose to the other radiosensitive organs including hippocampus involved in cognitive function of patients.

Keywords: scalp sparing; glioblastoma; IMRT; VMAT; neural structures.

*Corresponding author; *e-mail*: calinb2003@yahoo.com

1. Introduction

Transient and permanent alopecia have a psychological impact on radio-treated patient's quality of life.

Brain tumors radiotherapy with hair follicle protection for alopecia reduction has become a viable option by introduction of the inverse planning radiotherapy techniques. Limmer *et al.* has been demonstrating the potential to reduce the scalp dose in the whole brain treatment of brain metastases, by helical tomotherapy from 10 years ago, confirming data from the treatment planning system TPS using thermo-luminescent dosimetry (TLD). In the case of high-grade gliomas, reducing alopecia by protecting the scalp is often difficult due to the presence of the target volume in the vicinity of the scalp (Limmer *et al.*, 2007).

The purpose of the study is to evaluate the possibility of inverse planning techniques to reduce the dose to the scalp to reduce alopecia of patients and to assess the dosimetric consequences of applying these constraints on the other OARs.

2. Materials and Methods

For 3 patients with a pathologic diagnosis of glioblastoma multiform (GBM) surgically resected and proposed for adjuvant radiotherapy, CT simulation was performed using a Siemens Somatom AS simulator. The patients were immobilized using a thermoplastic mask system and CT simulation image were reconstructed in 3 mm slice thickness (Fuller *et al.*, 2007).

6 alternative treatment plans were proposed for each patient: 2 plans using 3D-CRT (3D conformal) technique, 6 MV or 10 MV energy with 4-7 non-coplanar fields, 2 by IMRT (intensity modulated radiation therapy) technique using 4-7 coplanar fields, 6 MV energy and 2 VMAT (volumetric modulated arc therapy) plans using 2 complete arcs and 6MV energy. Dose prescription for target volume was 60Gy/30 fractions. For all plans, dosimetric constraints for OARs were applied according to the QUANTEC guidelines (quantitative analysis of normal tissue effects in the clinic). For the scalp, dosimetric constraint was applied only for one of the IMRT plans and one of the VMAT plans (0% dose of the scalp <35Gy).

The gross tumor volume (GTV) was delineated using an image fusion and a rigid registration algorithm. The surgical bed delineated using preoperative MRI and the contrast enhanced lesion (identified on postoperative T1-weighted MRI) were included. The clinical target volume (CTV) was defined by adding an isotropic 2-cm margin to the GTV and was edited according to the anatomical barriers. For the planning target volume (PTV), CTV was expanded with 5 mm. Brain, brain stem, optic nerves, hippocampus,

eyes and lenses were delineated as organs at risk (OARs). Whole scalp from the surface of the scalp skin to the depth of the cranium was delineated as OAR (Dobbs *et al.*, 2009; Song *et al.*, 2015).

For glioblastoma cases, the most common primary brain tumor, a net benefit in survival has been proven with post-operative radiation therapy (RT) concurrent with temozolomide (TMZ) for 30 days followed by adjuvant TMZ treatment for another 6 months. Dose escalation above these values did not benefit in survival but increased the risk of toxicity (Barani and Larson, 2015).

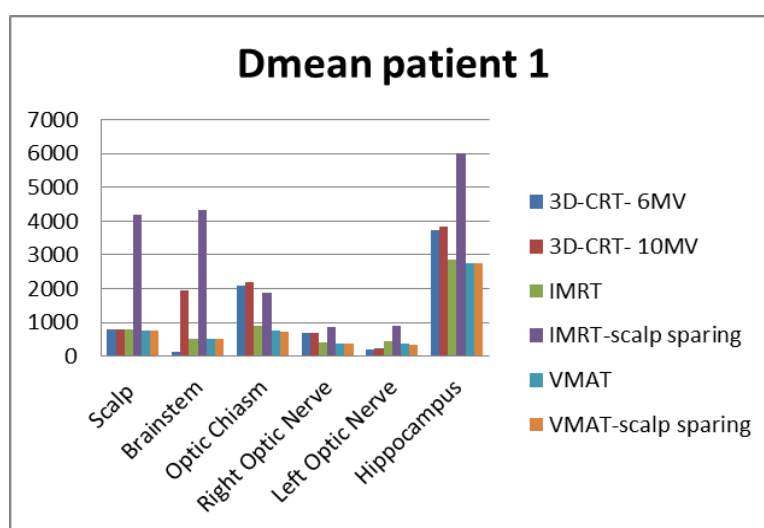


Fig. 1 – OARs mean dose for patient 1 for the five irradiation techniques.

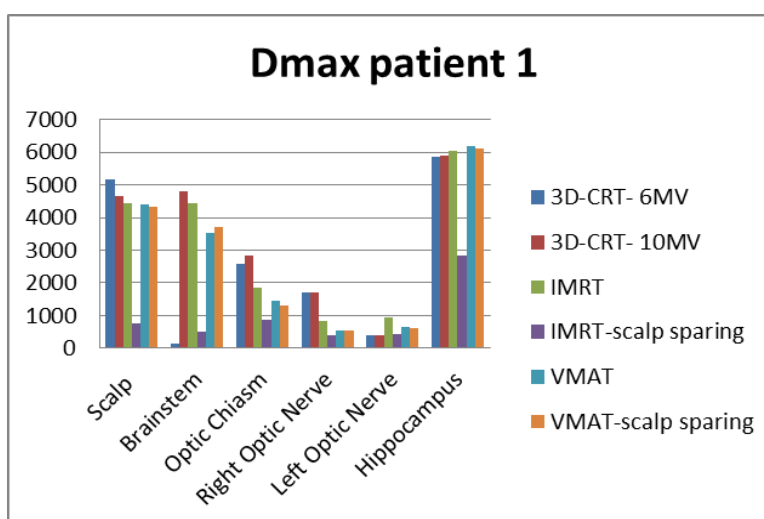


Fig. 2 – OARs maximum dose for patient 1 for the five irradiation techniques.

3. Results

In all three cases the application of a dosimetric constraint on the scalp did not lead to unpredictable increases in mean and maximum doses for other OARs. Hippocampus doses were comparable to those obtained without constraint or lower in some situations. For scalp, the IMRT technique reduced Dmean by 5.5%, 3.2% and 12.5% and Dmax by 18.7%, 9.6% and 8.3% for all three cases compared to the doses obtained using 3D-CRT (6MV energy) technique considered the standard treatment. The VMAT technique reduced Dmean with 5.1%, 0.8% and 22.2% and Dmax with 16.35, 11% and 16% relative to the 3D-CRT (6MV) radiotherapy plans (Figs. 1-6).

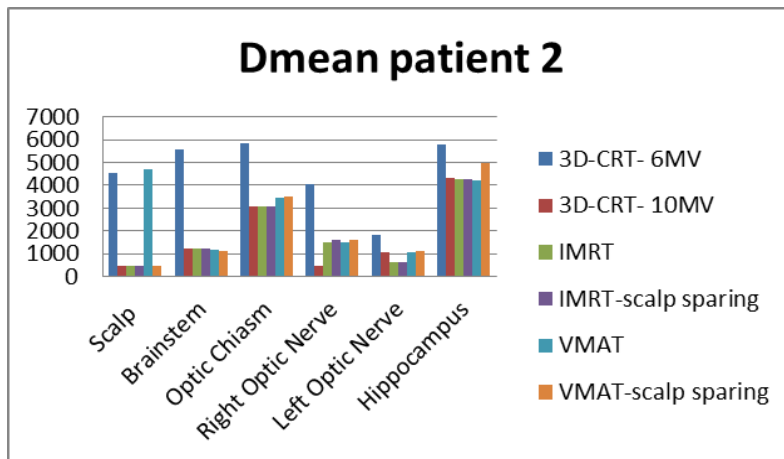


Fig. 3 – OARs mean dose for patient 2 for the five irradiation techniques.

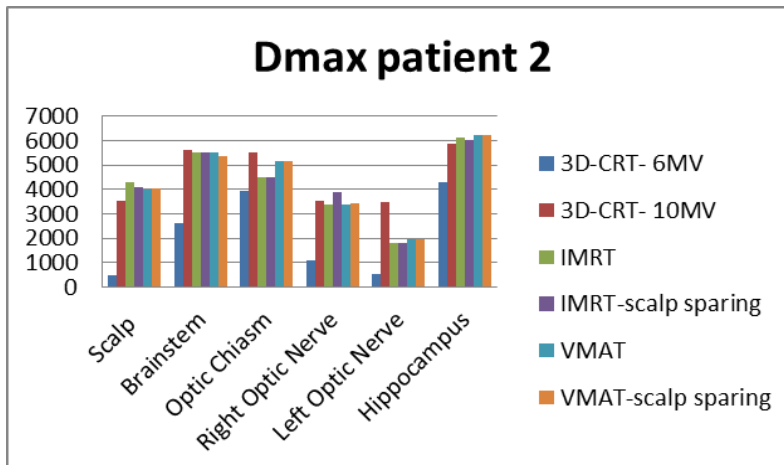


Fig. 4 – OARs maximum dose for patient 2 for the five irradiation techniques.

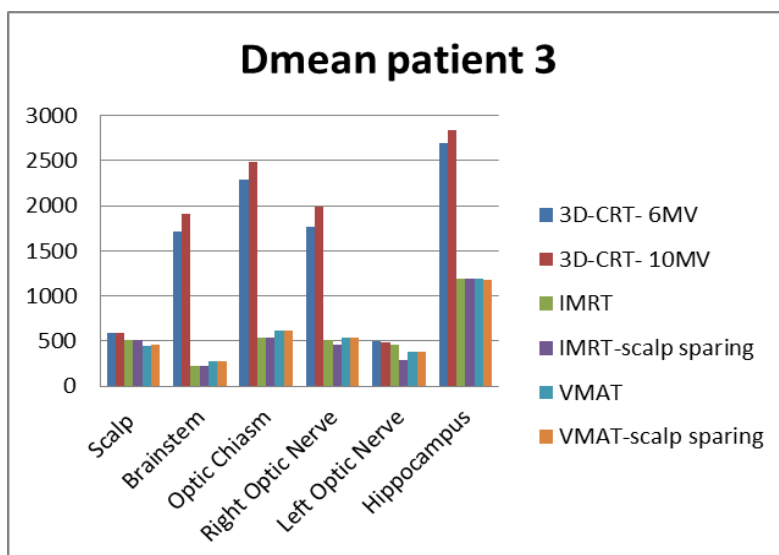


Fig. 5 – OARs mean dose for patient 3 for the five irradiation techniques.

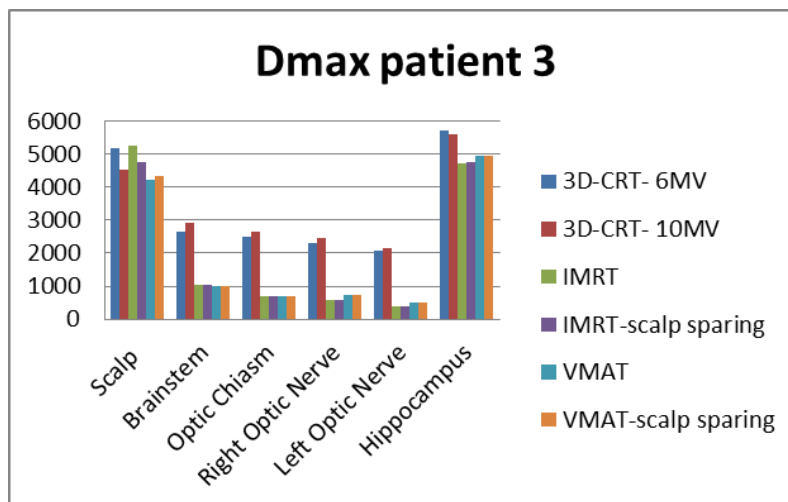


Fig. 6 – OARs maximum dose for patient 3 for the five irradiation techniques.

4. Discussion

Compared to the lateral opposed fields whole brain radiotherapy (OF-WBRT), the VMAT computations clearly predict a mean dose decrease of approximately 25% in the total hair follicle volume. Dose measurements demonstrated the potential of VMAT-WBRT to reduce the subcutaneously

absorbed dose by 20.5%. Roberge *et al.*, for comparison, measured a dose reduction of 53% at 1 mm depth with TLD's and calculated a dose reduction of 38% within the first 5 mm of the skin when comparing IMRT to OF-WBRT (De Puyseleyn *et al.*, 2014).

When compared to traditional opposed lateral fields, the IMRT plan with combined hippocampal and scalp-sparing constraints was able to significantly reduce the max and mean scalp dose as well as the percentage of scalp receiving 10 and 20Gy by 46% and 35%, respectively, while maintaining acceptable RTOG 0933 hippocampal dose variations. Witek *et al.* concluded that acceptable PTV coverage and sparing of the scalp and hippocampus can be obtained using a 9-field non-coplanar IMRT plan. No significant difference in hippocampal doses between the hippocampal-sparing and hippocampal-scalp-sparing plan was found using IMRT. IMRT was able to reduce the average measured dose to scalp by 53% from 95% of the prescription dose with the conventional plan to 44% with the IMRT plan (Witek *et al.*, 2014).

Three field IMRT plans were compared with conventional WBRT plans for 17 irradiated patients for brain metastases. IMRT reduced the mean scalp dose (26.2Gy vs. 16.4Gy, $p < 0.001$) and is a feasible technique to reduce alopecia in brain radiotherapy (Kao *et al.*, 2015).

Scoccianti *et al.* reports that a $D_{max} \leq 35\text{Gy}$ constraint was obtained in all cases using helical tomography, maintaining under the recommended dose limits at OARs but meeting the constraints for the scalp is not always possible for high grade gliomas targets that need to be treated with a total dose of 60Gy (Scoccianti *et al.*, 2016).

5. Conclusions

Applying a dosimetric constraint on the scalp, the doses D_{mean} and D_{max} may be reduced using IMRT and VMAT techniques compared to 3D-CRT radiotherapy (considered standard for brain tumors) without increasing the dose to the other OARs. For the hippocampus, the dosimetric evaluation has confirmed that scalp-sparing radiotherapy decreases in most cases or maintains comparable doses for hippocampus and this method can not lead to increased risk of cognitive impairment. The possibility to apply the technique in clinical practice should be evaluated on a larger number of patients and factors such as tumor volume and anatomical localization should be considered.

REFERENCES

- Barani I.J., Larson D.A., *Radiation Therapy of Glioblastoma*, Cancer Treat. Res., **163**, 49-73 (2015).
- De Puyssseleyr A., Van De Velde J., Speleers B. *et al.*, *Hair-Sparing Whole Brain Radiotherapy with Volumetric Arc Therapy in Patients Treated for Brain Metastases: Dosimetric and Clinical Results of a Phase II Trial*, Radiat. Oncol., **9**, 170 (2014).
- Dobbs J.E., Barrett A., Roques T., *Practical Radiotherapy Planning*, Fourth Edition, Boca Raton, Florida, CRC Press (2009).
- Fuller C.D., Choi M., Forthuber B., *Standard Fractionation Intensity Modulated Radiation Therapy (IMRT) of Primary and Recurrent Glioblastoma Multiforme*, Radiat. Oncol., **2**, 26 (2007).
- Kao J., Darakchiev B., Conboy L., *Tumor Directed, Scalp Sparing Intensity Modulated Whole Brain Radiotherapy for Brain Metastases*, Technol. Cancer Res. Treat., Oct., **14**, 5, 547-55 (2015).
- Limmer J.P., Buskerud J., Henrich D., *Scalp and Ear Sparing Whole Brain Radiation Therapy Using Helical Tomotherapy*, Int. J. Radiat. Oncol. Biol. Phys., Nov. 1, **69**, 3, S729 (2007).
- Scoccianti S., Simontacchi G., Talamonti C. *et al.*, *Scalp-Sparing Focal Radiotherapy for Gliomas Using VMAT or Helical Tomotherapy: A Feasibility Study*, Radiother. Oncol., Apr., **119**, 1, S778 (2016).
- Song J.H., Jung J.Y., Park H.W. *et al.*, *Dosimetric Comparison of Three Different Treatment Modalities for Total Scalp Irradiation: The Conventional Lateral Photon–Electron Technique, Helical Tomotherapy, and Volumetric-Modulated Arc Therapy*, J. Radiat. Res., Jul., **56**, 4, 717-726 (2015).
- Witek M. *et al.*, *Dose Reduction to the Scalp with Hippocampal Sparing is Achievable with Intensity Modulated Radiotherapy*, International Journal of Medical Physics, Clinical Engineering and Radiation Oncology, **3**, 176-182 (2014).

EFFECTUL DOZIMETRIC ASUPRA STRUCTURILOR
NEURONALE ALE RADIOTERAPIEI IMRT ȘI VMAT CARE PROTEJEAZĂ
SCALPUL ÎN CAZUL GLIOAMELOR DE GRAD ÎNALT

(Rezumat)

Radioterapia tumorilor cerebrale, cu protecția foliculilor piloși pentru reducerea alopeciei a devenit o opțiune viabilă odată cu introducerea tehnicilor de radioterapie cu planificare inversă. Scopul studiului a fost, evaluarea pe 3 cazuri de glioblastom temporo-parietal iradiat cu doza totală $DT = 60\text{Gy}$, posibilității reducerii dozei maxime și dozei medii permise de foliculii piloși și evaluarea consecințelor

dozimetrică asupra celorlalte organe la risc. În toate cele 3 cazuri s-a obținut pentru scalp o reducere a dozelor medii cu 5,5%, 3,2% și 12,5% prin tehnica IMRT și cu 5,1%, 0,8% și 22,2% prin tehnica VMAT. În cazul dozei maxime s-a obținut o scădere cu 18,7%, 9,6% și 8,3% prin tehnica IMRT și cu 16,35%, 11% și 16% prin tehnica VMAT fără a crește doza la celelalte organe la risc (inclusive hipocampul implicat în menținerea statusului cognitiv al pacienților).

BULETINUL INSTITUTULUI POLITEHNIC DIN IAȘI
Publicat de
Universitatea Tehnică „Gheorghe Asachi” din Iași
Volumul 63 (67), Numărul 4, 2017
Secția
MATEMATICĂ. MECANICĂ TEORETICĂ. FIZICĂ

**THE EFFECT OF DOSE ESCALATION AND OF THE SIZE OF
THE TARGET VOLUME ON LATE RECTAL TOXICITY RISK
IN ADVANCED LOCALIZED PROSTATE CANCER**

BY

**ALINA ROGOJANU¹, ALEXANDRU ZARA¹, CAMIL CIPRIAN MIREȘTEAN¹,
CĂLIN GHEORGHE BUZEA^{1,*} and DRAGOȘ TEODOR IANCU^{1,2}**

¹Regional Institute of Oncology, Iași

²“Grigore T. Popa” University of Medicine and Pharmacy, Iași

Received: October 23, 2017

Accepted for publication: December 22, 2017

Abstract. Radical prostatectomy or high-dose (definitive) radiotherapy are different options of curative treatment in patients with locally advanced prostate cancer. With the help of the Van Herk formula, one can define for each radiotherapy department CTV to PTV margin, taking into account the systematic and random errors occurred during the treatment implementation. These uncertainties setup margin calculated with this method guarantee that there is a 90% probability that 99% of the CTV is covered correctly. The CTV-PTV margins are recommended by the guidelines for every tumor localization but this margin may be reduced or increased depending on the possibilities of ensuring the reproducibility of the treatment in each radiotherapy department. The purpose of this study was to evaluate the effect on OAR of dose escalation up to 80Gy on the target prostate volume and the expansion of the prostate's PTV by 1, 2 and 3 mm. The potential risk of toxicity, particularly late rectal toxicity, has been evaluated.

Keywords: radical prostatectomy; dose escalation; prostate volume expansion; late rectal toxicity; radiotherapy.

*Corresponding author; *e-mail*: calinb2003@yahoo.com

1. Introduction

Radical prostatectomy or high-dose (definitive) radiotherapy (RT) are 2 options of curative treatment in patients with locally advanced prostate cancer.

The use of a more accurate tumor localization by including advanced imaging methods in the radiotherapy treatment plans and also the use of image guided radiation therapy IGRT for position reproducibility during the treatment have led to improved radiotherapy quality. Greater treatment precision would allow a reduction in CTV-PTV margins and the conforming of the planning target volume (PTV) more closely to the clinical target volume (CTV), in order to reduce the volume of healthy unnecessarily irradiated tissue. As a result, doses can be escalated without increasing the risk of toxicity, with local control and survival improvement clinically proven (Zietman *et al.*, 2005).

2. Materials and Methods

Each patient underwent CT simulation in supine position. Target volume and organs at risk (bladder, rectum, femoral heads) were delineated on 3mm slices CT simulation. The planning target volume include the prostate + seminal vesicles, with a 10 mm additional margin in each direction, except posteriorly where the margin was 5 mm in order to reduce rectum dose. According to the GETUG recommendations IGRT was associated with IMRT treatment. The total dose delivered to the prostate was 74Gy, respectively 56Gy and 46Gy for seminal vesicular and pelvic lymph nodes in standard fractionation.

Five patients with locally advanced prostate cancer were selected for this planning study. Patients were placed in a supine position and they were asked to keep their rectum empty. A protocol to fill the bladder with 500 mL of water before simulating after pre-emptying the bladder at the time of simulation and during treatment has also been used to control the filling of the bladder.

The recommendation of International Commission on Radiation Units and Measurements (ICRU 50 Report) were followed for delineation of the OAR and target volumes.

All plans were generated using 6 MV photons with five coplanar fields. A dosimetric guideline from the Royal Marsden NHS Trust allowed to receive 65Gy, 70Gy, and 75Gy for 30%, 15%, and 3%, respectively of entire rectum volumes (Clark *et al.*, 2002; Odrazka *et al.*, 2005).

Daily kV imaging for position verification and correction were performed prior to each treatment session.

The study of Ye and collaborators proves that by using of kV imaging and prostate fiducial markers to reproduce the position mean shifts in the inferior and superior directions were significantly greater, whereas AP and left-

right shifts did not differ as compared to the positioning with the aid of kV using bony landmarks. CBCT (cone-beam CT) positioning brings theoretical benefits through the ability to better locate of soft tissue landmarks but the is potentially more important when patient's bladder and rectum size vary significantly during the treatment (Ye *et al.*, 2015).

Barney *et al.* evaluated CBCT-guided IGRT, comparing it to kV portal image-guided fiducial alignment. And find that 60% of shift differences between the two positioning methods were greater than 3.0 mm, the authors endorsed fiducial alignment based on CBCT-related increases in treatment time because of repositioning by the physician based on soft tissue alignment. The time of CBCT images acquisition is not without consequences, studies proving the need to increase CTV-PTV margins by prolonging intrafractional treatment time (Barney *et al.*, 2011).

For 333 patients treated with external beam radiotherapy, 285 patients treated with radical radiotherapy and 48 patients postoperative radio-treated, rectal toxicity was related to the mean rectal dose and with anticoagulant/antiplatelet therapy with no differences in toxicity profile (Martinez-Arribas *et al.*, 2017).

In a retrospective study including 277 treated with 70Gy (10.8%), 74Gy (63.9%) and 80Gy (25.3%) using IMRT without pelvic irradiation rectal toxicity according to CTCA (Common Terminology Criteria for Adverse Events) version 4.0 was analyzed. The radiation doses of 80Gy is associated with a greater long-term grade ≥ 2 rectal toxicity but grade 3 toxicities were low for IMRT radiotherapy (6.2%) (Jolnerovski *et al.*, 2017).

3. Results

For the IMRT prostate plans with prescribed dose of 74Gy only 12 of the 20 proposed plans met the condition $V_{65} < 17\%$ and only 8, 5 and 4 plans for 76Gy, 78Gy and 80Gy respectively. Only for 4 IMRT treatment plans V_{40} was $< 35\%$. For the 74Gy prescription for which optimized plans were made for each target volume, prostate PTV expansion by 1mm increased average V_{65} by 7.32% V_{40} by 3.17% relative to the reference plane. Expansion of 2 mm and 3 mm increased average V_{65} by 7.04% and 8.25% respectively and V_{40} by 3.06% and 5.33% respectively. Dose escalation at 76Gy 78Gy and 80Gy plan optimizations led to an increased average V_{65} with 7.52%, 7.87% and 8.07% and an increased average V_{40} with 4.3%, 4.37% and 4.73% for the plan with prostate PTV expanded by 1mm. For PTV + 2mm, V_{65} values were increased by 7.69%, 8.12% and 8.39% and V_{40} values increased by 4.26%, 5.54% and 4.82%. If the planning was performed on a 3 mm expanded prostate PTV, V_{65} increased by 8.65%, 9.1% and 9.46% and V_{40} increased by 5.14%, 5.44% and 5.74% (Figs. 1 and 2).

For the rectum, Dmax was obtained with a maximum increase of 8.38% and Dmean with a maximum of 10.04% higher by combining the escalation of the dose and prostate PTV expansion. For the other OARs (bladder, femoral heads), isotropic expansion of PTV and dose escalation leads in most of the proposed treatment plans to an increase of Dmax and Dmean, proportional to the PTV volume and to the escalated prescribed dose. The effect is visible for optimized plans with isotropic expansion of the target volume for which in isolated cases lower values were obtained after replanning and for non-optimized plans by simply escalating the prescribed dose (Figs. 3-10).

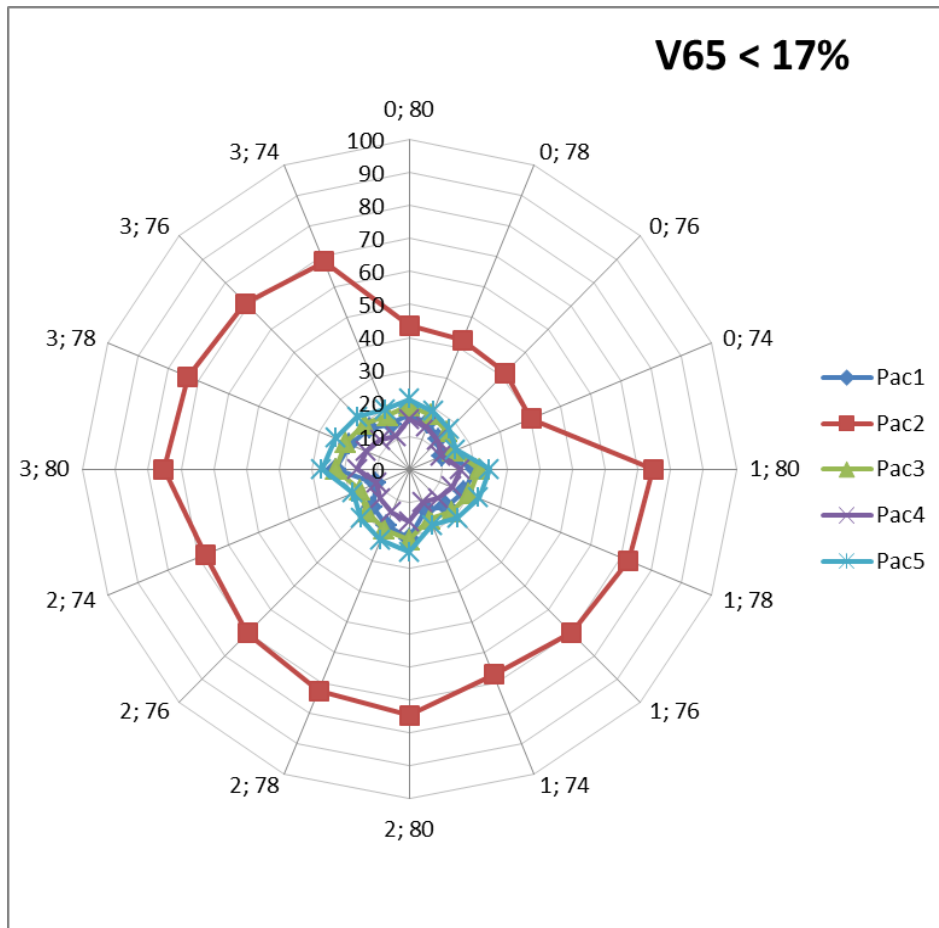


Fig. 1 – V65 chart for isotropic expansion of PTV and dose escalation. Note the labels of the rays mean (PTV expansion; dose escalation value).

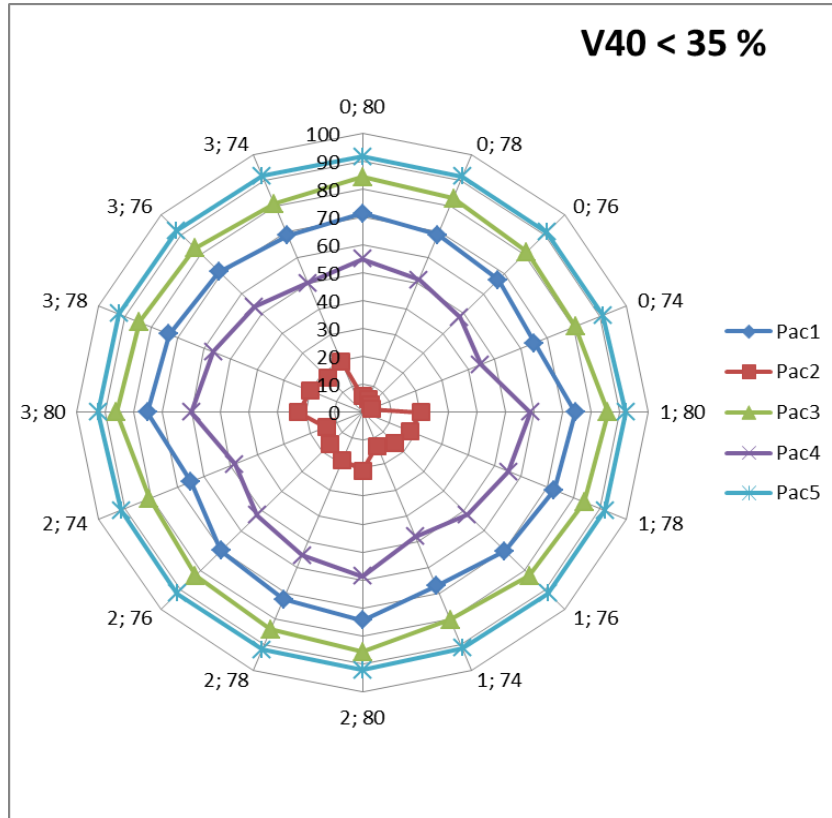


Fig. 2 – V40 chart for isotropic expansion of PTV and dose escalation. Note the labels of the rays mean (PTV expansion; dose escalation value).

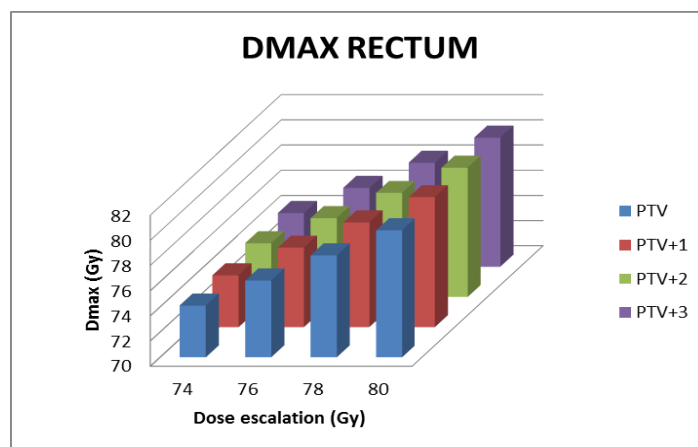


Fig. 3 – Dmax variation for isotropic expansion of PTV and dose escalation in rectum.

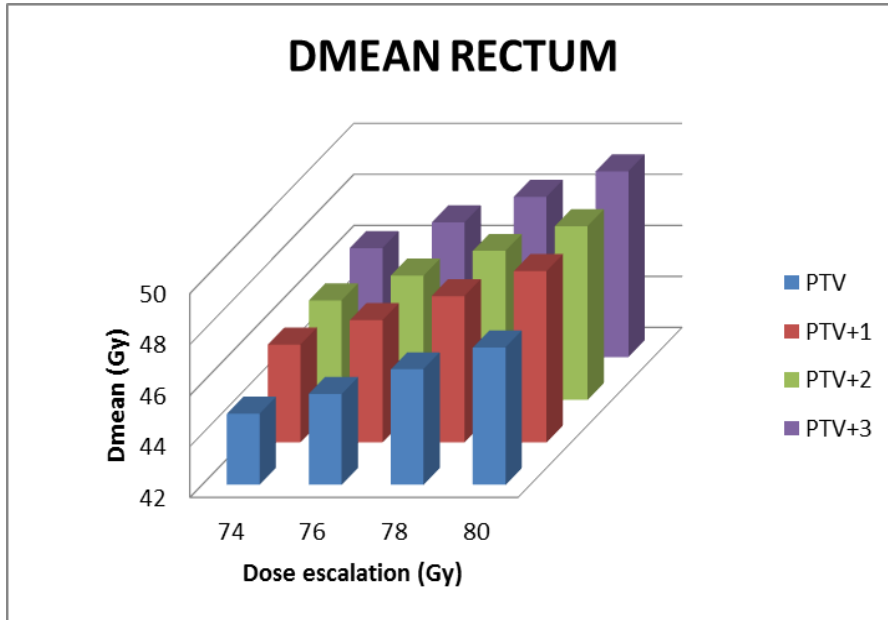


Fig. 4 – Dmean variation for isotropic expansion of PTV and dose escalation in rectum.

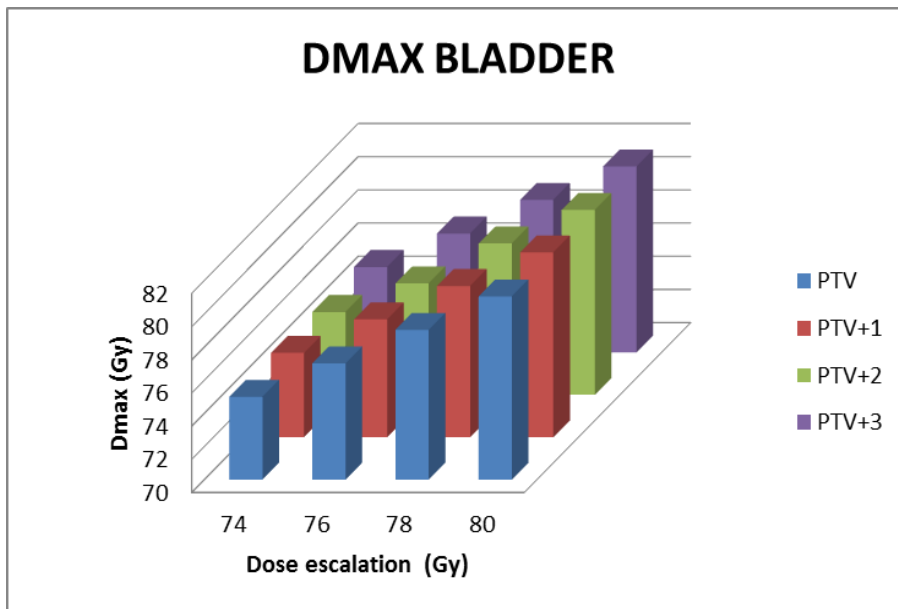


Fig. 5 – Dmax variation for isotropic expansion of PTV and dose escalation in bladder.

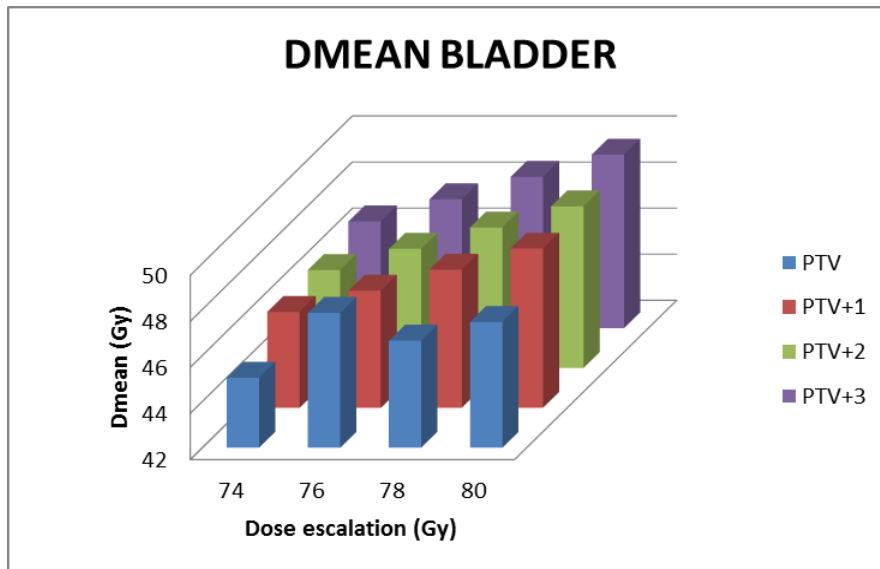


Fig. 6 – Dmean variation for isotropic expansion of PTV and dose escalation in bladder.

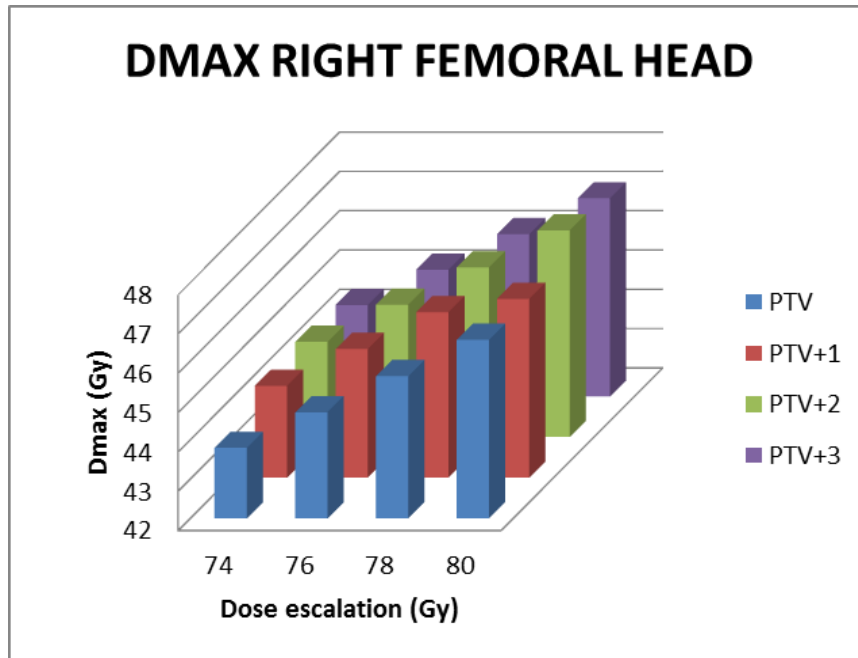


Fig. 7 – Dmax variation for isotropic expansion of PTV and dose escalation in right femoral head.

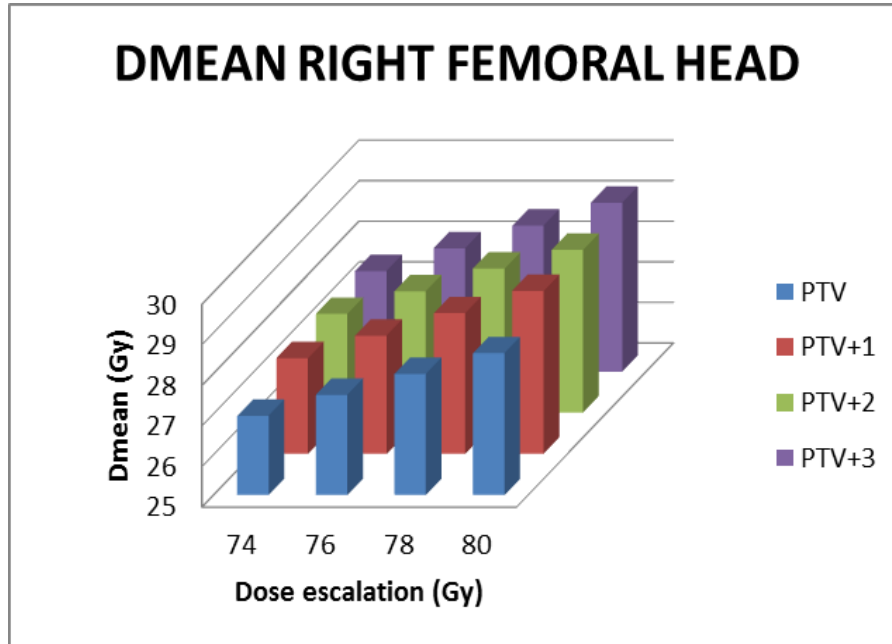


Fig. 8 – Dmean variation for isotropic expansion of PTV and dose escalation in right femoral head.

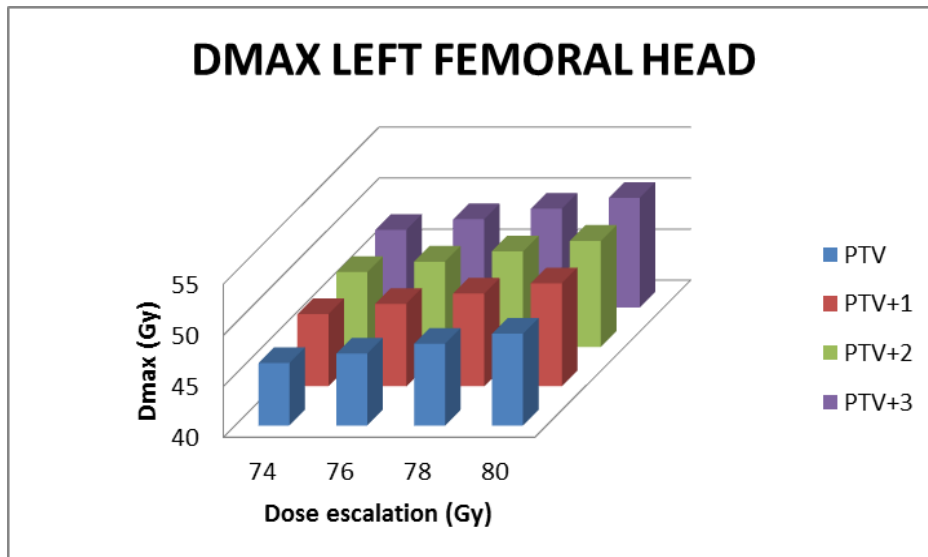


Fig. 9 – Dmax variation for isotropic expansion of PTV and dose escalation in left femoral head.

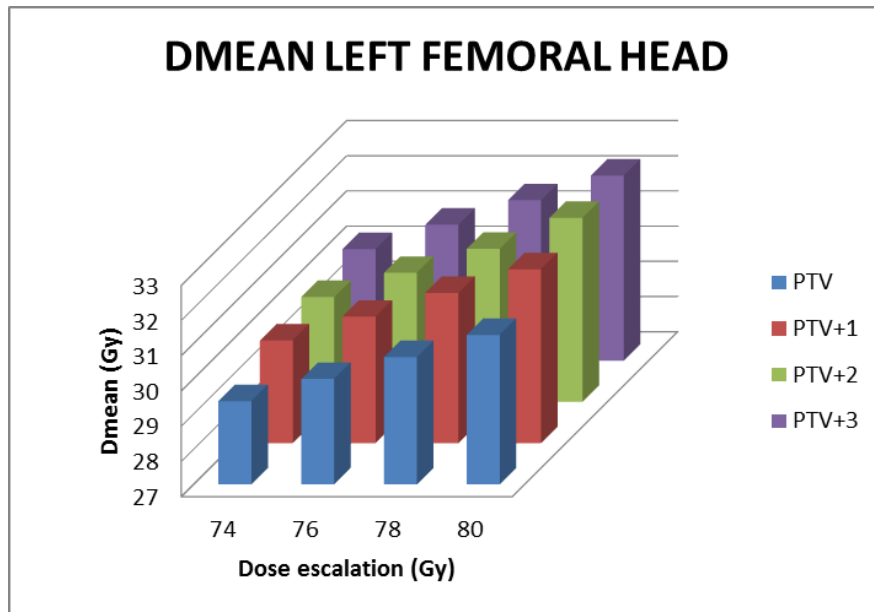


Fig. 10 – Dmean variation for isotropic expansion of PTV and dose escalation in left femoral head.

4. Conclusions

The unpredictable dose distribution and the steep dose gradient leads to the idea that the QUANTEC dosimetric recommendations for the rectum ($V_{50} < 50\%$, $V_{60} < 35\%$, $V_{65} < 25\%$, $V_{70} < 20\%$, $V_{75} < 15\%$) may not be sufficient in modern inverse planning radiotherapy techniques. Validation of additional constraints in the context of dose escalation for definitive treatment of locally advanced prostate cancers becomes necessary. Expansion of PTV due to increased uncertainty in patient set-up margin CTV-PTV for the prostate target can increase the risk of late rectal toxicity.

REFERENCES

- Barney B.M., Lee R.J., Handrahan D., Welsh K.T., Cook J.T., Sause W.T., *Image-Guided Radiotherapy (IGRT) for Prostate Cancer Comparing kV Imaging of Fiducial Markers with Cone Beam Computed Tomography (CBCT)*, Int. J. Radiat. Oncol. Biol. Phys., **80**, 301-305 (2011).
- Clark C.H., Mubata C.D., Meehan C.A. *et al.*, *IMRT Clinical Implementation: Prostate and Pelvic Irradiation Using Helios and a 120-Leaf Multileaf Collimator*, J. Appl. Clin. Med. Phys., **3**, 273-284 (2002).

- Jolnerovski M., Salleron J., Beckendorf V. *et al.*, *Intensity-Modulated Radiation Therapy from 70Gy to 80Gy in Prostate Cancer: Six- Year Outcomes and Predictors of Late Toxicity*, *Radiat. Oncol.*, Jun. 16, **12**, 1, 99 (2017).
- Martínez-Arribas C.M., González-San Segundo C., Cuesta-Álvaro P., *Predictors of Urinary and Rectal Toxicity After External Conformal Radiation Therapy in Prostate Cancer: Correlation Between Clinical, Tumour and Dosimetric Parameters and Radical and Postoperative Radiation Therapy*, *Actas. Urol. Esp.*, Jun. 15, pii: S0210-4806(17)30098-0 (2017).
- Odrzka K., Zouhar M., Petera J. *et al.*, *Comparison of Rectal Dose-Volume Constraints for IMRT Prostate Treatment Planning*, *Phys. Med.*, October-December, **21**, 4, 129-135 (2005).
- Ye J.C., Qureshi M.M., Clancy P. *et al.*, *Daily Patient Setup Error in Prostate Image Guided Radiation Therapy with Fiducial-Based Kilovoltage Onboard Imaging and Conebeam Computed Tomography*, *Quant. Imaging Med. Surg.*, Oct., **5**, 5, 665–672 (2015).
- Zietman A.L., DeSilvio M.L., Slater J.D. *et al.*, *Comparison of Conventional Dose vs. High-Dose Conformal Radiation Therapy in Clinically Localized Adenocarcinoma of the Prostate: A Randomized Controlled Trial*, *JAMA*, **294**, 1233-1239 (2005).

EFFECTUL ESCALADĂRII DOZEI ȘI A DIMENSIUNII VOLUMULUI ȚINTĂ
ASUPRA RISCULUI DE TOXICITATE RECTALĂ TARDIVĂ ÎN RADIOTERAPIA
NEOPLASMELOR DE PROSTATĂ LOCAL AVANSATE

(Rezumat)

Prostatectomia radicală sau radioterapia definitivă sunt 2 opțiuni de tratament curativ pentru pacienții cu cancer de prostată local avansat. Cu ajutorul formulei Van Herk's se pot defini pentru fiecare department de radioterapie marginea de la CTV la PTV ținând cont de erorile sistematice și aleatorii apărute pe parcursul implementării tratamentului. Această zonă de incertitudine adăugată izotrop la CTV asigură o probabilitate de 90% ca 99% din CTV să fie iradiat corespunzător. Marginile CTV-PTV recomandate de ghiduri au valoare orientativă, în fiecare departament ele putând fi reduse sau crescute în funcție de posibilitățile de asigurare a reproductibilității tratamentului. Scopul studiului a fost evaluarea efectului asupra OAR, în special asupra riscului toxicității rectale tardive escaladării dozelor până la 80Gy pe volumul țintă al prostatei și al expandării volumului PTV al prostatei cu câte 1 mm. S-a evaluat riscul potențial de toxicitate, în particular toxicitatea rectală tardivă.

BULETINUL INSTITUTULUI POLITEHNIC DIN IAȘI
Publicat de
Universitatea Tehnică „Gheorghe Asachi” din Iași
Volumul 63 (67), Numărul 4, 2017
Secția
MATEMATICĂ. MECANICĂ TEORETICĂ. FIZICĂ

EXISTENCE OF POSITIVE SOLUTIONS FOR A FRACTIONAL BOUNDARY VALUE PROBLEM

BY

RODICA LUCA*

“Gheorghe Asachi” Technical University of Iași,
Department of Mathematics

Received: November 25, 2017

Accepted for publication: December 10, 2017

Abstract. We study the existence and multiplicity of positive solutions for a system of nonlinear Riemann-Liouville fractional differential equations with nonnegative and nonsingular nonlinearities, subject to multi-point boundary conditions which contain fractional derivatives.

Keywords: Riemann-Liouville fractional differential equations; multi-point boundary conditions; positive solutions; existence; multiplicity.

1. Introduction

Fractional differential equations describe many phenomena in several fields of engineering and scientific disciplines such as physics, biophysics, chemistry, biology (for example, the primary infection with HIV), economics, control theory, signal and image processing, thermoelasticity, aerodynamics, viscoelasticity, electromagnetics and rheology (Arafa *et al.*, 2012; Baleanu *et al.*, 2012; Cole, 1993; Das, 2008; Ding and Ye, 2009; Djordjevic *et al.*, 2003; Ge and Ou, 2008; Kilbas *et al.*, 2006; Klafter *et al.*, 2011; Metzler and Klafter, 2000; Ostoja-Starzewski, 2007; Podlubny, 1999; Povstenko, 2015; Sabatier *et al.*, 2007; Samko *et al.*, 1993; Sokolov *et al.*, 2002). Fractional differential

*Corresponding author; *e-mail*: rluca@math.tuiasi.ro

equations are also regarded as a better tool for the description of hereditary properties of various materials and processes than the corresponding integer order differential equations.

We consider the system of nonlinear ordinary fractional differential equations

$$(S) \quad \begin{cases} D_{0+}^{\alpha} u(t) + f(t, u(t), v(t)) = 0, & t \in (0, 1), \\ D_{0+}^{\beta} v(t) + g(t, u(t), v(t)) = 0, & t \in (0, 1), \end{cases}$$

with the multi-point boundary conditions

$$(BC) \quad \begin{cases} u^{(j)}(0) = 0, & j = 0, \dots, n-2; & D_{0+}^{p_1} u(t)|_{t=1} = \sum_{i=1}^N a_i D_{0+}^{q_1} u(t)|_{t=\xi_i}, \\ v^{(j)}(0) = 0, & j = 0, \dots, m-2; & D_{0+}^{p_2} v(t)|_{t=1} = \sum_{i=1}^M b_i D_{0+}^{q_2} v(t)|_{t=\eta_i}, \end{cases}$$

where $\alpha, \beta \in \mathbb{R}$, $\alpha \in (n-1, n]$, $\beta \in (m-1, m]$, $n, m \in \mathbb{N}$, $n, m \geq 3$, $p_1, p_2, q_1, q_2 \in \mathbb{R}$, $p_1 \in [1, n-2]$, $p_2 \in [1, m-2]$, $q_1 \in [0, p_1]$, $q_2 \in [0, p_2]$, $\xi_i, \alpha_i \in \mathbb{R}$ for all $i = 1, \dots, N$ ($N \in \mathbb{N}$), $0 < \xi_1 < \dots < \xi_N \leq 1$, $\eta_i, b_i \in \mathbb{R}$ for all $i = 1, \dots, M$ ($M \in \mathbb{N}$), $0 < \eta_1 < \dots < \eta_M \leq 1$, and D_{0+}^k denotes the Riemann-Liouville derivative of order k (for $k = \alpha, \beta, p_1, p_2, q_1, q_2$).

Under sufficient conditions on the nonnegative and nonsingular functions f and g , we study the existence and multiplicity of positive solutions of problem (S)-(BC). We use some theorems from the fixed point index theory (Amann, 1976; Zhou and Xu, 2006). By a positive solution of problem (S)-(BC) we mean a pair of functions $(u, v) \in (C([0, 1], [0, \infty)))^2$ satisfying (S) and (BC) with $u(t) > 0$ for all $t \in (0, 1]$ or $v(t) > 0$ for all $t \in (0, 1]$.

The system (S) with some positive parameters, subject to the boundary conditions (BC) was investigated in (Henderson *et al.*, 2017). The system (S) with $f(t, u, v) = \tilde{f}(t, v)$, $g(t, u, v) = \tilde{g}(t, u)$ has been studied in (Henderson and Luca, 2017c). In this last paper, the authors use some different operators and different assumptions than those we use in this paper. The existence of positive solutions of the system (S) with the coupled multi-point boundary conditions

$$(\widetilde{BC}) \quad \begin{cases} u^{(j)}(0) = 0, & j = 0, \dots, n-2; & D_{0+}^{p_1} u(t)|_{t=1} = \sum_{i=1}^N a_i D_{0+}^{q_1} v(t)|_{t=\xi_i}, \\ v^{(j)}(0) = 0, & j = 0, \dots, m-2; & D_{0+}^{p_2} v(t)|_{t=1} = \sum_{i=1}^M b_i D_{0+}^{q_2} u(t)|_{t=\eta_i}, \end{cases}$$

was studied in (Henderson and Luca, 2017b). For other papers which investigate the existence, nonexistence and multiplicity of positive solutions for systems of fractional differential equations with nonnegative or sign-changing nonlinearities, subject to various nonlocal boundary conditions we mention (Henderson and Luca, 2014a, b; Luca and Tudorache, 2014; Henderson and Luca, 2015; Henderson *et al.*, 2015; Henderson and Luca, 2016a, b).

The paper is organized as follows. In Section 2, we present some auxiliary results which investigate a nonlocal boundary value problem for fractional differential equations, and we give the properties of the Green

functions associated to our problem. Section 3 contains the existence and multiplicity results for the positive solutions of problem (S)-(BC).

2. Auxiliary Results

We present here some auxiliary results from (Henderson and Luca, 2017a) that will be used to prove our main results.

We consider the fractional differential equation

$$D_{0+}^{\alpha}u(t) + x(t) = 0, \quad 0 < t < 1, \tag{1}$$

with the multi-point boundary conditions

$$u^{(j)}(0) = 0, \quad j = 0, \dots, n - 2; \quad D_{0+}^{p_1}u(t)|_{t=1} = \sum_{i=1}^N a_i D_{0+}^{q_1}u(t)|_{t=\xi_i}, \tag{2}$$

where $\alpha \in (n - 1, n], n \in \mathbb{N}, n \geq 3, a_i, \xi_i \in \mathbb{R}, i = 1, \dots, N (N \in \mathbb{N}),$

$0 < \xi_1 < \dots < \xi_N \leq 1, p_1, q_1 \in \mathbb{R}, p_1 \in [1, n - 2], q_1 \in [0, p_1],$ and

$x \in C(0,1) \cap L^1(0,1).$ We denote by $\Delta_1 = \frac{\Gamma(\alpha)}{\Gamma(\alpha-p_1)} - \frac{\Gamma(\alpha)}{\Gamma(\alpha-q_1)} \sum_{i=1}^N a_i \xi_i^{\alpha-q_1-1}.$

Lemma 1. *If $\Delta_1 \neq 0,$ then the function $u \in C[0,1]$ given by*

$$u(t) = \int_0^1 G_1(t, s)x(s)ds, \quad t \in [0,1], \tag{3}$$

is solution of problem (1)-(2), where

$$G_1(t, s) = g_1(t, s) + \frac{t^{\alpha-1}}{\Delta_1} \sum_{i=1}^N a_i g_2(\xi_i, s), \quad \forall (t, s) \in [0,1] \times [0,1], \tag{4}$$

and

$$g_1(t, s) = \frac{1}{\Gamma(\alpha)} \begin{cases} t^{\alpha-1}(1-s)^{\alpha-p_1-1} - (t-s)^{\alpha-1}, & 0 \leq s \leq t \leq 1, \\ t^{\alpha-1}(1-s)^{\alpha-p_1-1}, & 0 \leq t \leq s \leq 1, \end{cases} \tag{5}$$

$$g_2(t, s) = \frac{1}{\Gamma(\alpha - q_1)} \begin{cases} t^{\alpha-q_1-1}(1-s)^{\alpha-p_1-1} - (t-s)^{\alpha-q_1-1}, & 0 \leq s \leq t \leq 1, \\ t^{\alpha-q_1-1}(1-s)^{\alpha-p_1-1}, & 0 \leq t \leq s \leq 1. \end{cases}$$

Lemma 2. *The functions g_1 and g_2 given by (5) have the properties:*

a) $g_1(t, s) \leq h_1(s)$ for all $t, s \in [0,1],$ where

$$h_1(s) = \frac{1}{\Gamma(\alpha)} (1-s)^{\alpha-p_1-1} (1 - (1-s)^{p_1}), \quad s \in [0,1];$$

b) $g_1(t, s) \geq t^{\alpha-1}h_1(s)$ for all $t, s \in [0,1];$

c) $g_1(t, s) \leq \frac{t^{\alpha-1}}{\Gamma(\alpha)}$ for all $t, s \in [0,1];$

d) $g_2(t, s) \geq t^{\alpha-q_1-1}h_2(s)$ for all $t, s \in [0,1],$ where

$$h_2(s) = \frac{1}{\Gamma(\alpha - q_1)} (1-s)^{\alpha-p_1-1} (1 - (1-s)^{p_1-q_1}), \quad s \in [0,1];$$

e) $g_2(t, s) \leq \frac{1}{\Gamma(\alpha - q_1)} t^{\alpha-q_1-1}$ for all $t, s \in [0,1];$

- f) The functions g_1 and g_2 are continuous on $[0,1] \times [0,1]$; $g_1(t,s) \geq 0$, $g_2(t,s) \geq 0$ for all $t,s \in [0,1]$; $g_1(t,s) > 0$, $g_2(t,s) > 0$ for all $t,s \in (0,1)$.

Lemma 3. Assume that $a_i \geq 0$ for all $i = 1, \dots, N$ and $\Delta_1 > 0$. Then the function G_1 given by (4) is a nonnegative continuous function on $[0,1] \times [0,1]$ and satisfies the inequalities:

- a) $G_1(t,s) \leq J_1(s)$ for all $t,s \in [0,1]$, where

$$J_1(s) = h_1(s) + \frac{1}{\Delta_1} \sum_{i=1}^N a_i g_2(\xi_i, s), \quad s \in [0,1];$$

- b) $G_1(t,s) \geq t^{\alpha-1} J_1(s)$ for all $t,s \in [0,1]$;

- c) $G_1(t,s) \leq \sigma_1 t^{\alpha-1}$, for all $t,s \in [0,1]$, where

$$\sigma_1 = \frac{1}{\Gamma(\alpha)} + \frac{1}{\Delta_1 \Gamma(\alpha-q_1)} \sum_{i=1}^N a_i \xi_i^{\alpha-q_1-1}.$$

Lemma 4. Assume that $a_i \geq 0$ for all $i = 1, \dots, N$, $\Delta_1 > 0$, $x \in C(0,1) \cap L^1(0,1)$ and $x(t) \geq 0$ for all $t \in (0,1)$. Then the solution u of problem (1)-(2) given by (3) satisfies the inequality $u(t) \geq t^{\alpha-1} u(t')$ for all $t, t' \in [0,1]$.

We can also formulate similar results as Lemmas 1-4 for the fractional boundary value problem

$$D_{0+}^{\beta} v(t) + y(t) = 0, \quad 0 < t < 1, \quad (6)$$

$$v^{(j)}(0) = 0, \quad j = 0, \dots, m-2; \quad D_{0+}^{p_2} v(t)|_{t=1} = \sum_{i=1}^M b_i D_{0+}^{q_2} v(t)|_{t=\eta_i}, \quad (7)$$

where $\beta \in (m-1, m]$, $m \in \mathbb{N}$, $m \geq 3$, $b_i, \eta_i \in \mathbb{R}$, $i = 1, \dots, M$ ($M \in \mathbb{N}$),

$0 < \eta_1 < \dots < \eta_M \leq 1$, $p_2, q_2 \in \mathbb{R}$, $p_2 \in [1, m-2]$, $q_2 \in [0, p_2]$ and $y \in C(0,1) \cap L^1(0,1)$.

We denote by $\Delta_2, g_3, g_4, G_2, h_3, h_4, J_2$ and σ_2 the corresponding constants and functions for problem (6)-(7) defined in a similar manner as $\Delta_1, g_1, g_2, G_1, h_1, h_2, J_1$ and σ_1 , respectively. More precisely, we have

$$\begin{aligned} \Delta_2 &= \frac{\Gamma(\beta)}{\Gamma(\beta-p_2)} - \frac{\Gamma(\beta)}{\Gamma(\beta-q_2)} \sum_{i=1}^M b_i \eta_i^{\beta-q_2-1}, \\ g_3(t,s) &= \frac{1}{\Gamma(\beta)} \begin{cases} t^{\beta-1} (1-s)^{\beta-p_2-1} - (t-s)^{\beta-1}, & 0 \leq s \leq t \leq 1, \\ t^{\beta-1} (1-s)^{\beta-p_2-1}, & 0 \leq t \leq s \leq 1, \end{cases} \\ g_4(t,s) &= \frac{1}{\Gamma(\beta-q_2)} \begin{cases} t^{\beta-q_2-1} (1-s)^{\beta-p_2-1} - (t-s)^{\beta-q_2-1}, & 0 \leq s \leq t \leq 1, \\ t^{\beta-q_2-1} (1-s)^{\beta-p_2-1}, & 0 \leq t \leq s \leq 1, \end{cases} \\ G_2(t,s) &= g_3(t,s) + \frac{t^{\beta-1}}{\Delta_2} \sum_{i=1}^M b_i g_4(\eta_i, s), \quad \forall (t,s) \in [0,1] \times [0,1], \\ h_3(s) &= \frac{1}{\Gamma(\beta)} (1-s)^{\beta-p_2-1} (1 - (1-s)^{p_2}), \quad s \in [0,1], \end{aligned}$$

$$h_4(s) = \frac{1}{\Gamma(\beta - q_2)} (1-s)^{\beta-p_2-1} (1 - (1-s)^{p_2-q_2}), \quad s \in [0,1],$$

$$J_2(s) = h_3(s) + \frac{1}{\Delta_2} \sum_{i=1}^M b_i g_4(\eta_i, s), \quad s \in [0,1],$$

$$\sigma_2 = \frac{1}{\Gamma(\beta)} + \frac{1}{\Delta_2 \Gamma(\beta - q_2)} \sum_{i=1}^M b_i \eta_i^{\beta-q_2-1}.$$

The inequalities from Lemmas 3 and 4 for the functions G_2 and v are the following $G_2(t, s) \leq J_2(s)$, $G_2(t, s) \geq t^{\beta-1} J_2(s)$, $G_2(t, s) \leq \sigma_2 t^{\beta-1}$, for all $t, s \in [0,1]$, and $v(t) \geq t^{\beta-1} v(t')$ for all $t, t' \in [0,1]$.

Remark 1. Under the assumptions of Lemma 4, and of the corresponding lemma for problem (6)-(7), for $c \in (0,1)$, the solutions u, v of problems (1)-(2) and (6)-(7), respectively, satisfy the inequalities

$$\begin{aligned} \min_{t \in [c,1]} u(t) &\geq c^{\alpha-1} \max_{t' \in [0,1]} u(t'), \\ \min_{t \in [c,1]} v(t) &\geq c^{\beta-1} \max_{t' \in [0,1]} v(t'). \end{aligned}$$

The proofs of our results are based on the following fixed point index theorems. Let E be a real Banach space, $P \subset E$ a cone, “ \leq ” the partial ordering defined by P and θ the zero element in E . For $\varrho > 0$, let $B_\varrho = \{u \in E, \|u\| < \varrho\}$ be the open ball of radius ϱ centered at θ , and its boundary $\partial B_\varrho = \{u \in E, \|u\| = \varrho\}$.

Theorem 1. (Amann, 1976) Let $A: \bar{B}_\varrho \cap P \rightarrow P$ be a completely continuous operator which has no fixed point on $\partial B_\varrho \cap P$. If $\|Au\| \leq \|u\|$ for all $u \in \partial B_\varrho \cap P$, then $i(A, B_\varrho \cap P, P) = 1$.

Theorem 2. (Amann, 1976) Let $A: \bar{B}_\varrho \cap P \rightarrow P$ be a completely continuous operator. If there exists $u_0 \in P \setminus \{\theta\}$ such that $u - Au \neq \lambda u_0$, for all $\lambda \geq 0$ and $u \in \partial B_\varrho \cap P$, then $i(A, B_\varrho \cap P, P) = 0$.

Theorem 3. (Zhou and Xu, 2006) Let $A: \bar{B}_\varrho \cap P \rightarrow P$ be a completely continuous operator which has no fixed point on $\partial B_\varrho \cap P$. If there exists a linear operator $L: P \rightarrow P$ and $u_0 \in P \setminus \{\theta\}$ such that

$$i) u_0 \leq Lu_0, \quad ii) Lu \leq Au, \quad \forall u \in \partial B_\varrho \cap P,$$

then $i(A, B_\varrho \cap P, P) = 0$.

3. Main Results

In this section we investigate the existence and multiplicity of positive solutions for problem (S)-(BC) under various assumptions on the functions f and g .

We present the assumptions that we shall use in the sequel.

(H1) $\alpha, \beta \in \mathbb{R}$, $\alpha \in (n-1, n]$, $\beta \in (m-1, m]$, $n, m \in \mathbb{N}$, $n, m \geq 3$,
 $p_1, p_2, q_1, q_2 \in \mathbb{R}$, $p_1 \in [1, n-2]$, $p_2 \in [1, m-2]$, $q_1 \in [0, p_1]$, $q_2 \in [0, p_2]$,
 $\xi_i \in \mathbb{R}$, $a_i \geq 0$ for all $i = 1, \dots, N$ ($N \in \mathbb{N}$), $0 < \xi_1 < \dots < \xi_N \leq 1$, $\eta_i \in \mathbb{R}$,
 $b_i \geq 0$ for all $i = 1, \dots, M$ ($M \in \mathbb{N}$), $0 < \eta_1 < \dots < \eta_M \leq 1$, $\Delta_1 = \frac{\Gamma(\alpha)}{\Gamma(\alpha-p_1)} -$
 $\frac{\Gamma(\alpha)}{\Gamma(\alpha-q_1)} \sum_{i=1}^N a_i \xi_i^{\alpha-q_1-1} > 0$, $\Delta_2 = \frac{\Gamma(\beta)}{\Gamma(\beta-p_2)} - \frac{\Gamma(\beta)}{\Gamma(\beta-q_2)} \sum_{i=1}^M b_i \eta_i^{\beta-q_2-1} > 0$.

(H2) The functions $f, g: [0,1] \times [0, \infty) \times [0, \infty) \rightarrow [0, \infty)$ are continuous.

By using Lemma 2, a solution of the following nonlinear system of integral equations

$$\begin{cases} u(t) = \int_0^1 G_1(t,s) f(s, u(s), v(s)) ds, & t \in [0,1], \\ v(t) = \int_0^1 G_2(t,s) g(s, u(s), v(s)) ds, & t \in [0,1] \end{cases}$$

is solution of problem (S)-(BC).

We consider the Banach space $X = C[0,1]$ with supremum norm $\|\cdot\|$ and the Banach space $Y = X \times X$ with the norm $\|(u, v)\|_Y = \|u\| + \|v\|$. We define the cone $P \subset Y$ by $P = \{(u, v) \in Y, u(t) \geq 0, v(t) \geq 0 \text{ for all } t \in [0,1]\}$.

We introduce the operators $Q_1, Q_2: Y \rightarrow X$ and $Q: Y \rightarrow Y$ defined by

$$Q_1(u, v)(t) = \int_0^1 G_1(t,s) f(s, u(s), v(s)) ds, \quad t \in [0,1],$$

$$Q_2(u, v)(t) = \int_0^1 G_2(t,s) g(s, u(s), v(s)) ds, \quad t \in [0,1],$$

and $Q(u, v) = (Q_1(u, v), Q_2(u, v))$, $(u, v) \in Y$.

Under the assumptions (H1) and (H2), it is easy to see that operator $Q: P \rightarrow P$ is completely continuous. It is obvious that if (u, v) is a fixed point of operator Q , then (u, v) is a solution of problem (S)-(BC). Therefore, we will study the existence and multiplicity of fixed points of operator Q .

Theorem 4. Assume that (H1) and (H2) hold. If the functions f and g also satisfy the conditions

(H3) There exist $p \geq 1$ and $q \geq 1$ such that

$$f_0^s = \lim_{u+v \rightarrow 0} \sup_{u, v \geq 0} \sup_{t \in [0,1]} \frac{f(t, u, v)}{(u+v)^p} = 0 \quad \text{and}$$

$$g_0^s = \lim_{u+v \rightarrow 0} \sup_{u, v \geq 0} \sup_{t \in [0,1]} \frac{g(t, u, v)}{(u+v)^q} = 0;$$

(H4) There exists $c \in (0,1)$ such that

$$f_\infty^i = \lim_{u+v \rightarrow \infty} \inf_{u, v \geq 0} \inf_{t \in [c,1]} \frac{f(t, u, v)}{u+v} = \infty \quad \text{and}$$

$$g_\infty^i = \lim_{u+v \rightarrow \infty} \inf_{u, v \geq 0} \inf_{t \in [c,1]} \frac{g(t, u, v)}{u+v} = \infty,$$

then problem (S)-(BC) has at least one positive solution $(u(t), v(t))$, $t \in [0,1]$.

Proof. For c given in (H4) we define the cone

$$P_0 = \left\{ (u, v) \in P, \quad \min_{t \in [c, 1]} u(t) \geq c^{\alpha-1} \|u\|, \quad \min_{t \in [c, 1]} v(t) \geq c^{\beta-1} \|v\| \right\}.$$

From our assumptions and Remark 1, for any $(u, v) \in P$, we deduce that $Q(u, v) = (Q_1(u, v), Q_2(u, v)) \in P_0$, that is $Q(P) \subset P_0$.

We consider the functions $u_0, v_0: [0, 1] \rightarrow \mathbb{R}$ defined by

$$u_0(t) = \int_0^1 G_1(t, s) ds, \quad v_0(t) = \int_0^1 G_2(t, s) ds, \quad t \in [0, 1],$$

that is (u_0, v_0) is solution of problem (1)-(2) with $x(t) = x_0(t)$, $y(t) = y_0(t)$, $x_0(t) = 1$, $y_0(t) = 1$ for all $t \in [0, 1]$. Hence $(u_0, v_0) = Q(x_0, y_0) \in P_0$.

We define the set

$$\tilde{M} = \{ (u, v) \in P,$$

there exists $\lambda \geq 0$ such that $(u, v) = Q(u, v) + \lambda(u_0, v_0)$ }. $\}$

We will show that $\tilde{M} \subset P_0$ and \tilde{M} is a bounded set of Y . If $(u, v) \in \tilde{M}$, then there exists $\lambda \geq 0$ such that $(u, v) = Q(u, v) + \lambda(u_0, v_0)$ or equivalently

$$\begin{cases} u(t) = \int_0^1 G_1(t, s) (f(s, u(s), v(s)) + \lambda) ds, & t \in [0, 1], \\ v(t) = \int_0^1 G_2(t, s) (g(s, u(s), v(s)) + \lambda) ds, & t \in [0, 1]. \end{cases}$$

By Remark 1, we obtain $(u, v) \in P_0$, so $\tilde{M} \subset P_0$, and

$$\|u\| \leq \frac{1}{c^{\alpha-1}} \min_{t \in [c, 1]} u(t), \quad \|v\| \leq \frac{1}{c^{\beta-1}} \min_{t \in [c, 1]} v(t), \quad \forall (u, v) \in \tilde{M}. \quad (8)$$

From (H4) we have $f_\infty^i = \infty$ and $g_\infty^i = \infty$. Then for $\epsilon_1 = \frac{2}{c^{\alpha-1} m_1} > 0$,

$\epsilon_2 = \frac{2}{c^{\beta-1} m_2} > 0$, there exist $C_1 > 0$, $C_2 > 0$ such that

$$\begin{aligned} f(t, u, v) &\geq \epsilon_1(u + v) - C_1, & g(t, u, v) &\geq \epsilon_2(u + v) - C_2, \\ \forall (t, u, v) &\in [c, 1] \times [0, \infty) \times [0, \infty), \end{aligned} \quad (9)$$

where $m_i = \int_c^1 J_i(s) ds$ and J_i , $i = 1, 2$ are defined in Lemma 3.

For $(u, v) \in \tilde{M}$ and $t \in [c, 1]$, by using Lemma 3 and relations (9), we obtain

$$\begin{aligned} u(t) &= Q_1(u, v)(t) + \lambda u_0(t) \geq Q_1(u, v)(t) \\ &= \int_0^1 G_1(t, s) f(s, u(s), v(s)) ds \geq \int_c^1 t^{\alpha-1} J_1(s) f(s, u(s), v(s)) ds \\ &\geq c^{\alpha-1} \int_c^1 J_1(s) [\epsilon_1(u(s) + v(s)) - C_1] ds \\ &\geq c^{\alpha-1} \epsilon_1 \int_c^1 J_1(s) u(s) ds - c^{\alpha-1} m_1 C_1 \\ &\geq c^{\alpha-1} \epsilon_1 m_1 \min_{s \in [c, 1]} u(s) - c^{\alpha-1} m_1 C_1 \\ &\geq 2 \min_{s \in [c, 1]} u(s) - C_3, \quad C_3 = c^{\alpha-1} m_1 C_1, \end{aligned}$$

and

$$\begin{aligned} v(t) &= Q_2(u, v)(t) + \lambda v_0(t) \geq Q_2(u, v)(t) \\ &= \int_0^1 G_2(t, s) g(s, u(s), v(s)) ds \geq \int_c^1 t^{\beta-1} J_2(s) g(s, u(s), v(s)) ds \\ &\geq c^{\beta-1} \int_c^1 J_2(s) [\epsilon_2(u(s) + v(s)) - C_2] ds \\ &\geq c^{\beta-1} \epsilon_2 \int_c^1 J_2(s) v(s) ds - c^{\beta-1} m_2 C_2 \end{aligned}$$

$$\begin{aligned} &\geq c^{\beta-1} \epsilon_2 m_2 \min_{s \in [c,1]} v(s) - c^{\beta-1} m_2 C_2 \\ &\geq 2 \min_{s \in [c,1]} v(s) - C_4, \quad C_4 = c^{\beta-1} m_2 C_2. \end{aligned}$$

Therefore, we deduce

$$\min_{t \in [c,1]} u(t) \leq C_3, \quad \min_{t \in [c,1]} v(t) \leq C_4, \quad \forall (u, v) \in \tilde{M}. \quad (10)$$

Now from relations (8) and (10), we obtain

$$\begin{aligned} \|u\| &\leq \frac{C_3}{c^{\alpha-1}}, \quad \|v\| \leq \frac{C_4}{c^{\beta-1}}, \\ \|(u, v)\|_Y &= \|u\| + \|v\| \leq \frac{C_3}{c^{\alpha-1}} + \frac{C_4}{c^{\beta-1}} = C_5, \end{aligned}$$

for all $(u, v) \in \tilde{M}$, that is \tilde{M} is a bounded set of Y .

Besides, there exists a sufficiently large $R_1 > 1$ such that

$$(u, v) \neq Q(u, v) + \lambda(u_0, v_0), \quad \forall (u, v) \in \partial B_{R_1} \cap P, \quad \forall \lambda \geq 0.$$

From (Amann, 1976), we deduce that the fixed point index of operator Q over $B_{R_1} \cap P$ with respect to P is

$$i(Q, B_{R_1} \cap P, P) = 0. \quad (11)$$

Next, from assumption (H3), we conclude that for $\epsilon_3 = \frac{1}{4M_1} > 0$ and $\epsilon_4 = \frac{1}{4M_2} > 0$, there exists $r_1 \in (0,1]$ such that

$$\begin{aligned} f(t, u, v) &\leq \epsilon_3 (u + v)^p, \quad g(t, u, v) \leq \epsilon_4 (u + v)^q, \\ \forall t \in [0,1], \quad u, v &\geq 0, \quad u + v \leq r_1, \end{aligned} \quad (12)$$

where $M_i = \int_0^1 J_i(s) ds$, $i = 1, 2$.

By using (12), we deduce that for all $(u, v) \in \bar{B}_{r_1} \cap P$ and $t \in [0,1]$

$$\begin{aligned} Q_1(u, v)(t) &\leq \int_0^1 J_1(s) \epsilon_3 (u(s) + v(s))^p ds \\ &\leq \epsilon_3 M_1 \|(u, v)\|_Y^p \leq \frac{1}{4} \|(u, v)\|_Y, \\ Q_2(u, v)(t) &\leq \int_0^1 J_2(s) \epsilon_4 (u(s) + v(s))^q ds \\ &\leq \epsilon_4 M_2 \|(u, v)\|_Y^q \leq \frac{1}{4} \|(u, v)\|_Y. \end{aligned}$$

These imply that

$$\|Q_1(u, v)\| \leq \frac{1}{4} \|(u, v)\|_Y, \quad \|Q_2(u, v)\| \leq \frac{1}{4} \|(u, v)\|_Y,$$

$$\|Q(u, v)\|_Y = \|Q_1(u, v)\| + \|Q_2(u, v)\| \leq \frac{1}{2} \|(u, v)\|_Y, \quad \forall (u, v) \in \partial B_{r_1} \cap P.$$

From (Amann, 1976), we conclude that the fixed point index of operator Q over $B_{r_1} \cap P$ with respect to P is

$$i(Q, B_{r_1} \cap P, P) = 1. \quad (13)$$

Combining (11) and (13) we obtain

$$i(Q, (B_{R_1} \setminus \bar{B}_{r_1}) \cap P, P) = i(Q, B_{R_1} \cap P, P) - i(Q, B_{r_1} \cap P, P) = -1.$$

We deduce that Q has at least one fixed point $(u, v) \in (B_{R_1} \setminus \bar{B}_{r_1}) \cap P$,

that is $r_1 < \|(u, v)\|_Y < R_1$ or $r_1 < \|u\| + \|v\| < R_1$. By Lemma 4, we obtain that $u(t) > 0$ for all $t \in (0, 1]$ or $v(t) > 0$ for all $t \in (0, 1]$. The proof is completed. ■

Theorem 5. Assume that (H1) and (H2) hold. If the functions f and g also satisfy the conditions

$$(H5) \quad f_\infty^s = \lim_{\substack{u+v \rightarrow \infty \\ u, v \geq 0}} \sup_{t \in [0, 1]} \frac{f(t, u, v)}{u+v} = 0 \quad \text{and} \\ g_\infty^s = \lim_{\substack{u+v \rightarrow \infty \\ u, v \geq 0}} \sup_{t \in [0, 1]} \frac{g(t, u, v)}{u+v} = 0;$$

(H6) There exist $c \in (0, 1)$, $\hat{p} \in (0, 1]$ and $\hat{q} \in (0, 1]$ such that

$$f_0^i = \lim_{\substack{u+v \rightarrow 0 \\ u, v \geq 0}} \inf_{t \in [c, 1]} \frac{f(t, u, v)}{(u+v)^{\hat{p}}} = \infty \quad \text{and} \\ g_0^i = \lim_{\substack{u+v \rightarrow 0 \\ u, v \geq 0}} \inf_{t \in [c, 1]} \frac{g(t, u, v)}{(u+v)^{\hat{q}}} = \infty,$$

then problem (S)-(BC) has at least one positive solution $(u(t), v(t))$, $t \in [0, 1]$.

Proof. From the assumption (H5), we deduce that for $\epsilon_5 = \frac{1}{4M_1} > 0$ and

$\epsilon_6 = \frac{1}{4M_2} > 0$, there exist $C_6 > 0$, $C_7 > 0$ such that

$$f(t, u, v) \leq \epsilon_5(u + v) + C_6, \quad g(t, u, v) \leq \epsilon_6(u + v) + C_7, \quad (14) \\ \forall (t, u, v) \in [0, 1] \times [0, \infty) \times [0, \infty).$$

Hence for $(u, v) \in P$, by using (14), we obtain

$$Q_1(u, v)(t) \leq \int_0^1 J_1(s)(\epsilon_5(u(s) + v(s)) + C_6)ds \\ \leq \epsilon_5(\|u\| + \|v\|) \int_0^1 J_1(s)ds + C_6 \int_0^1 J_1(s)ds \\ = \epsilon_5 \|(u, v)\|_Y M_1 + C_6 M_1 = \frac{1}{4} \|(u, v)\|_Y + C_6 M_1, \quad \forall t \in [0, 1],$$

$$Q_2(u, v)(t) \leq \int_0^1 J_2(s)(\epsilon_6(u(s) + v(s)) + C_7)ds \\ \leq \epsilon_6(\|u\| + \|v\|) \int_0^1 J_2(s)ds + C_7 \int_0^1 J_2(s)ds \\ = \epsilon_6 \|(u, v)\|_Y M_2 + C_7 M_2 = \frac{1}{4} \|(u, v)\|_Y + C_7 M_2, \quad \forall t \in [0, 1],$$

and so

$$\|Q(u, v)\|_Y = \|Q_1(u, v)\| + \|Q_2(u, v)\| \leq \frac{1}{2} \|(u, v)\|_Y + (C_6 M_1 + C_7 M_2) \\ = \frac{1}{2} \|(u, v)\|_Y + C_8, \quad C_8 = C_6 M_1 + C_7 M_2.$$

Then there exists a sufficiently large $R_2 \geq \max\{4C_8, 1\}$ such that

$$\|Q(u, v)\|_Y \leq \frac{3}{4} \|(u, v)\|_Y, \quad \forall (u, v) \in P, \|(u, v)\|_Y \geq R_2.$$

Hence $\|Q(u, v)\|_Y < \|(u, v)\|_Y$ for all $(u, v) \in \partial B_{R_2} \cap P$ and from (Amann, 1976) we have

$$i(Q, B_{R_2} \cap P, P) = 1. \quad (15)$$

On the other hand, from (H6) we deduce that for $\epsilon_7 = \frac{1}{c^{\alpha-1} m_1} > 0$,

$\epsilon_8 = \frac{1}{c^{\beta-1} m_2} > 0$, there exists $r_2 \in (0, 1)$ such that

$$f(t, u, v) \geq \epsilon_7(u+v)^{\hat{p}}, \quad g(t, u, v) \geq \epsilon_8(u+v)^{\hat{q}}, \quad (16)$$

$$\forall t \in [c, 1], \quad u, v \geq 0, \quad u+v \leq r_2.$$

From (16), we deduce that for any $(u, v) \in \bar{B}_{r_2} \cap P$

$$\begin{aligned} Q_1(u, v)(t) &\geq \int_c^1 G_1(t, s) f(s, u(s), v(s)) ds \\ &\geq \int_c^1 \epsilon_7 G_1(t, s) (u(s) + v(s))^{\hat{p}} ds \\ &\geq \epsilon_7 \int_c^1 G_1(t, s) (u(s) + v(s)) ds =: L_1(u, v)(t), \quad \forall t \in [0, 1], \\ Q_2(u, v)(t) &\geq \int_c^1 G_2(t, s) g(s, u(s), v(s)) ds \\ &\geq \int_c^1 \epsilon_8 G_2(t, s) (u(s) + v(s))^{\hat{q}} ds \\ &\geq \epsilon_8 \int_c^1 G_2(t, s) (u(s) + v(s)) ds =: L_2(u, v)(t), \quad \forall t \in [0, 1]. \end{aligned}$$

Hence

$$Q(u, v) \geq L(u, v), \quad \forall (u, v) \in \partial B_{r_2} \cap P, \quad (17)$$

where the linear operator $L: P \rightarrow P$ is defined by $L(u, v) = (L_1(u, v), L_2(u, v))$.

For $(\tilde{u}_0, \tilde{v}_0) \in P \setminus \{(0, 0)\}$ defined by

$$\tilde{u}_0(t) = \int_c^1 G_1(t, s) ds, \quad \tilde{v}_0(t) = \int_c^1 G_2(t, s) ds, \quad \forall t \in [0, 1],$$

we have $L(\tilde{u}_0, \tilde{v}_0) = (L_1(\tilde{u}_0, \tilde{v}_0), L_2(\tilde{u}_0, \tilde{v}_0))$ with

$$\begin{aligned} L_1(\tilde{u}_0, \tilde{v}_0)(t) &= \epsilon_7 \int_c^1 G_1(t, s) \left(\int_c^1 G_1(s, \tau) d\tau + \int_c^1 G_2(s, \tau) d\tau \right) ds \\ &\geq \epsilon_7 \int_c^1 G_1(t, s) \left(\int_c^1 G_1(s, \tau) d\tau \right) ds \\ &\geq \epsilon_7 \int_c^1 G_1(t, s) \left(\int_c^1 c^{\alpha-1} J_1(\tau) d\tau \right) ds \\ &= \epsilon_7 c^{\alpha-1} m_1 \int_c^1 G_1(t, s) ds = \int_c^1 G_1(t, s) ds = \tilde{u}_0(t), \quad \forall t \in [0, 1], \\ L_2(\tilde{u}_0, \tilde{v}_0)(t) &= \epsilon_8 \int_c^1 G_2(t, s) \left(\int_c^1 G_1(s, \tau) d\tau + \int_c^1 G_2(s, \tau) d\tau \right) ds \\ &\geq \epsilon_8 \int_c^1 G_2(t, s) \left(\int_c^1 G_2(s, \tau) d\tau \right) ds \\ &\geq \epsilon_8 \int_c^1 G_2(t, s) \left(\int_c^1 c^{\beta-1} J_2(\tau) d\tau \right) ds \\ &= \epsilon_8 c^{\beta-1} m_2 \int_c^1 G_2(t, s) ds = \int_c^1 G_2(t, s) ds = \tilde{v}_0(t), \quad \forall t \in [0, 1]. \end{aligned}$$

So

$$L(\tilde{u}_0, \tilde{v}_0) \geq (\tilde{u}_0, \tilde{v}_0). \quad (18)$$

We may suppose that Q has no fixed point on $\partial B_{r_2} \cap P$ (otherwise the proof is finished). From (17), (18) and (Zhou and Xu, 2006, Lemma 3), we conclude that

$$i(Q, B_{r_2} \cap P, P) = 0. \quad (19)$$

Therefore, from (15) and (19), we have

$$i(Q, (B_{R_2} \setminus \bar{B}_{r_2}) \cap P, P) = i(Q, B_{R_2} \cap P, P) - i(Q, B_{r_2} \cap P, P) = 1.$$

Then Q has at least one fixed point in $(B_{R_2} \setminus \bar{B}_{r_2}) \cap P$, that is $r_2 < \|(u, v)\|_Y < R_2$. Thus problem (S)-(BC) has at least one positive solution $(u, v) \in P$. This completes the proof. \blacksquare

Theorem 6. Assume that (H1), (H2), (H4) and (H6) hold. If the functions f and g also satisfy the condition

(H7) For each $t \in [0,1]$, $f(t,u,v)$ and $g(t,u,v)$ are nondecreasing with respect to u and v , and there exists a constant $N_0 > 0$ such that

$$f(t, N_0, N_0) < \frac{N_0}{2m_0}, \quad g(t, N_0, N_0) < \frac{N_0}{2m_0}, \quad \forall t \in [0,1],$$

where $m_0 = \max\{M_i, i = 1,2\}$, ($M_i = \int_0^1 J_i(s)ds$, $i = 1,2$),

then problem (S)-(BC) has at least two positive solutions $(u_1(t), v_1(t))$, $(u_2(t), v_2(t))$, $t \in [0,1]$.

Proof. By using (H7), for any $(u, v) \in \partial B_{N_0} \cap P$, we obtain

$$\begin{aligned} Q_1(u, v)(t) &\leq \int_0^1 G_1(t, s) f(s, N_0, N_0) ds \leq \int_0^1 J_1(s) f(s, N_0, N_0) ds \\ &< \frac{N_0}{2m_0} \int_0^1 J_1(s) ds = \frac{N_0 M_1}{2m_0} \leq \frac{N_0}{2}, \quad \forall t \in [0,1], \end{aligned}$$

$$\begin{aligned} Q_2(u, v)(t) &\leq \int_0^1 G_2(t, s) g(s, N_0, N_0) ds \leq \int_0^1 J_2(s) g(s, N_0, N_0) ds \\ &< \frac{N_0}{2m_0} \int_0^1 J_2(s) ds = \frac{N_0 M_2}{2m_0} \leq \frac{N_0}{2}, \quad \forall t \in [0,1]. \end{aligned}$$

Then we deduce

$$\|Q(u, v)\|_Y = \|Q_1(u, v)\| + \|Q_2(u, v)\| < N_0, \quad \forall (u, v) \in \partial B_{N_0} \cap P.$$

By (Amann, 1976) we conclude that

$$i(Q, B_{N_0} \cap P, P) = 1. \quad (20)$$

On the other hand, from (H4) and (H6) and the proofs of Theorem 4 and Theorem 5, we know that there exists a sufficiently large $R_1 > N_0$ and a sufficiently small $r_2 \in (0, N_0)$ such that

$$i(Q, B_{R_1} \cap P, P) = 0, \quad i(Q, B_{r_2} \cap P, P) = 0, \quad (21)$$

From the relations (20) and (21), we obtain

$$i(Q, (B_{R_1} \setminus \bar{B}_{N_0}) \cap P, P) = i(Q, B_{R_1} \cap P, P) - i(Q, B_{N_0} \cap P, P) = -1,$$

$$i(Q, (B_{N_0} \setminus \bar{B}_{r_2}) \cap P, P) = i(Q, B_{N_0} \cap P, P) - i(Q, B_{r_2} \cap P, P) = 1.$$

Then Q has at least one fixed point $(u_1, v_1) \in (B_{R_1} \setminus \bar{B}_{N_0}) \cap P$ and has at least one fixed point $(u_2, v_2) \in (B_{N_0} \setminus \bar{B}_{r_2}) \cap P$. If in Theorem 5, the operator Q has at least one fixed point on $\partial B_{r_2} \cap P$, then by using the first relation from formula above, we deduce that Q has at least one fixed point $(u_1, v_1) \in (B_{R_1} \setminus \bar{B}_{N_0}) \cap P$ and has at least one fixed point $(u_2, v_2) \in \partial B_{r_2} \cap P$. Therefore, problem (S)-(BC) has two distinct positive solutions (u_1, v_1) , (u_2, v_2) . The proof is completed. ■

REFERENCES

- Amann H., *Fixed Point Equations and Nonlinear Eigenvalue Problems in Ordered Banach Spaces*, SIAM Review, **18**, 620-709 (1976).
- Arafa A.A.M., Rida S.Z., Khalil M., *Fractional Modeling Dynamics of HIV and CD4+ T-Cells During Primary Infection*, Nonlinear Biomed. Phys., **6**, 1, 1-7 (2012).
- Baleanu D., Diethelm K., Scalas E., Trujillo J.J., *Fractional Calculus Models and Numerical Methods. Series on Complexity, Nonlinearity and Chaos*, World Scientific, Boston, 2012.
- Cole K., *Electric Conductance of Biological Systems*, in: Proc. Cold Spring Harbor Symp. Quant. Biol., Col Springer Harbor Laboratory Press, New York, 1993, 107-116.
- Das S., *Functional Fractional Calculus for System Identification and Controls*, Springer, New York, 2008.
- Ding Y., Ye H., *A Fractional-Order Differential Equation Model of HIV Infection of CD4+ T-Cells*, Math. Comp. Model., **50**, 386-392 (2009).
- Djordjevic V., Jaric J., Fabry B., Fredberg J., Stamenovic D., *Fractional Derivatives Embody Essential Features of Cell Rheological Behavior*, Ann. Biomed. Eng., **31**, 692-699 (2003).
- Ge Z.M., Ou C.Y., *Chaos Synchronization of Fractional Order Modified Duffing Systems with Parameters Excited by a Chaotic Signal*, Chaos Solitons Fractals, **35**, 705-717 (2008).
- Henderson J., Luca R., *Existence and Multiplicity of Positive Solutions for a System of Fractional Boundary Value Problems*, Bound. Value Probl., **60**, 1-17 (2014a).
- Henderson J., Luca R., *Positive Solutions for a System of Fractional Differential Equations with Coupled Integral Boundary Conditions*, Appl. Math. Comput., **249**, 182-197 (2014b).
- Henderson J., Luca R., *Nonexistence of Positive Solutions for a System of Coupled Fractional Boundary Value Problems*, Bound. Value Probl., **138**, 1-12 (2015).
- Henderson J., Luca R., *Positive Solutions for a System of Semipositone Coupled Fractional Boundary Value Problems*, Bound. Value Probl., **61**, 1-23 (2016a).
- Henderson J., Luca R., *Boundary Value Problems for Systems of Differential, Difference and Fractional Equations. Positive Solutions*, Elsevier, Amsterdam, 2016b.
- Henderson J., Luca R., *Existence of Positive Solutions for a Singular Fractional Boundary Value Problem*, Nonlinear Anal. Model. Control, **22**, 1, 99-114 (2017a).
- Henderson J., Luca R., *Systems of Riemann-Liouville Fractional Equations with Multi-Point Boundary Conditions*, Appl. Math. Comput., **309**, 303-323 (2017b).
- Henderson J., Luca R., *Positive Solutions for a System of Fractional Boundary Value Problems*, in Proceedings of EQUADIFF 2017 Conference, Editors Karol Mikula, Daniel Sevcovic, Jozef Urban, Published by Slovak University of Technology, Publishing House, Bratislava, Slovakia, 2017c, 1-10.
- Henderson J., Luca R., Tudorache A., *On a System of Fractional Differential Equations with Coupled Integral Boundary Conditions*, Fract. Calc. Appl. Anal., **18**, 2, 361-386 (2015).

- Henderson J., Luca R., Tudorache A., *Positive Solutions for a System of Fractional Differential Equations with Multi-Point Boundary Conditions*, submitted (2017).
- Kilbas A.A., Srivastava H.M., Trujillo J.J., *Theory and Applications of Fractional Differential Equations*, North-Holland Mathematics Studies, 204, Elsevier Science B.V., Amsterdam, 2006.
- Klafter J., Lim S.C., Metzler R., *Fractional Dynamics in Physics*, Singapore, World Scientific, 2011.
- Luca R., Tudorache A., *Positive Solutions to a System of Semipositone Fractional Boundary Value Problems*, Adv. Difference Equ., **179**, 1-11 (2014).
- Metzler R., Klafter J., *The Random Walks Guide to Anomalous Diffusion: a Fractional Dynamics Approach*, Phys. Rep., **339**, 1-77 (2000).
- Ostoja-Starzewski M., *Towards Thermoelasticity of Fractal Media*, J. Therm. Stress., **30**, 889-896 (2007).
- Podlubny I., *Fractional Differential Equations*, Academic Press, San Diego, 1999.
- Povstenko Y.Z., *Fractional Thermoelasticity*, New York, Springer, 2015.
- Sabatier J., Agrawal O.P., Machado J.A.T., *Advances in Fractional Calculus: Theoretical Developments and Applications in Physics and Engineering*, Springer, Dordrecht, 2007.
- Samko S.G., Kilbas A.A., Marichev O.I., *Fractional Integrals and Derivatives. Theory and Applications*, Gordon and Breach, Yverdon, 1993.
- Sokolov I.M., Klafter J., Blumen A., *A Fractional Kinetics*, Phys. Today, **55**, 48-54 (2002).
- Zhou Y., Xu Y., *Positive Solutions of three-Point Boundary Value Problems for Systems of Nonlinear Second Order Ordinary Differential Equations*, J. Math. Anal. Appl., **320**, 578-590 (2006).

EXISTENȚA SOLUȚIILOR POZITIVE PENTRU O
PROBLEMĂ LA LIMITĂ FRAȚIONARĂ

(Rezumat)

Studiem existența și multiplicitatea soluțiilor pozitive pentru sistemul de ecuații diferențiale fracționare Riemann-Liouville (S) cu neliniarități nenegative și nesingulare, cu condițiile la limită (BC) cu mai multe puncte care conțin derivate fracționare.

BULETINUL INSTITUTULUI POLITEHNIC DIN IAȘI
Publicat de
Universitatea Tehnică „Gheorghe Asachi” din Iași
Volumul 63 (67), Numărul 4, 2017
Secția
MATEMATICĂ. MECANICĂ TEORETICĂ. FIZICĂ

LASER ABLATION: STATE OF THE ART AND PERSPECTIVES

BY

ȘTEFAN ANDREI IRIMICIUC* and BIANCA CRISTIANA HODOROABĂ

“Alexandru Ioan Cuza” University of Iași,
Faculty of Physics

Received: November 20, 2017

Accepted for publication: December 12, 2017

Abstract. Laser ablation community has seen a strong development in the past 20 years. This is related with the technological development of shorter laser beams and more flexible diagnostics systems. In this paper we focus on the fundamental mechanisms of laser ablation and state of the art in the matter of diagnostics methods and the complete picture that we now have over the laser ablation process and laser produced plasma dynamics.

Keywords: laser produced plasmas; fundamental ablation mechanism; Coulomb explosion.

1. Short History of Laser Ablation

Laser ablation is defining a series of processes that are the results of a laser beam impinge onto a solid surface. The effects of “photonic ablation” (or the interaction of photons with the matter) have been tentatively known for centuries. Some example can be found even in the Greek literature, when in 303 B.C. are presented the properties of a globe filled with water that can light fire, regardless of the environmental conditions. Also, the concept of “photonic ablation” is even mentioned by Archimedes, who proposed in 203 B.C. to reflect and focus the sunlight on the Phoenicians attacking the city using an array of mirrors (Miller, 1994).

*Corresponding author; *e-mail*: stefan.irimiciuc@yahoo.com

The “modern” history of the laser ablation started with a series of conference papers and talks from the 1960’s. The results reported in those papers covered a series of fundamental aspects that are considered as the pillars of laser ablation and laser-produced plasmas which led to the development of an entirely new research direction. The first recorded “regular” paper was a theoretical study of Askar'yan and Moroz (1963), where they made some calculations regarding the recoil pressure during the laser ablation of a solid target and discussed the acceleration of small particles or droplets in the framework of an "one-sided evaporation" model. They also predicted the presence of ultrasonic and hypersonic oscillations produced by modulated laser ablation. Following, in a similar pioneering experimental drive, Honig and Woolston (1963) reported some results from the investigation of laser ablation of various targets (metals, semiconductors and dielectrics). They reported for the first time a quantitative measurement of the ejected particles (3×10^{16} electrons and 10^8 positive ions per m^3). The published paper presented the first detailed study of the electron emission and its temporal profile. They analyzed the mass distribution with a modified commercial, double-focusing mass spectrometer, thus demonstrating the first use of the ion microprobe analysis. This study will further be the basis for ion mass spectrometry and paved the way for electrical investigations of LPPs. In later papers Lichtman and Ready (1963), using a simple assumption of thermionic emission, derived the temperature of the surface during laser-target interaction, finding values of about 3300 K for a ruby laser interaction with a tungsten target. Ready (1963) proved for the first time the implementation of high-speed photography as a viable method to study the temporal and spatial profiles of the plume of ejected material. The paper reported on a carbon laser ablation plasma. One of the main results presented in that paper was that the emitted light from the plasma reached its maximum at about 120 ns after the start of the laser pulse and had an estimated life-time of a few microseconds. From here, the expansion velocity of the plume was estimated as being of 20 km/s. Follow-up studies on carbon-based targets were performed by Howe (1963), who reported on the energy of the ejected particles by means of the vibrational (0.86 - 1.72 eV) and rotational (0.38 eV) temperatures extracted from fluorescence spectra of CN and C₂. This represents one of the first mentioning of possible non-equilibrium conditions that were attributed to the cooling of the ejected particles during an adiabatic expansion. This subject was further investigated by Berkowitz and Chupka (1964), who observed, after post-ionization of the ablated plume, cluster ions of carbon ($n \sim 14$), boron ($n \sim 5$) and manganese ($n \sim 2$). Exploring the production of large structures during laser ablation, there have been reports (Neuman, 1964) of large “blobs of molten material” and “fragments of material” suggested by the first momentum transfer measurements. This short period of time is characterized by a fast expansion of laser-matter interaction and related topics, during which the first reported papers concentrated on the study of

various properties of the ejected particles (electrons, ions, neutrals, clusters and emitted photons). This, coupled with the first estimations of plasma temperatures, velocities and densities, led to the formation of a coherent image of the complex processes involved in the laser-matter interaction.

In the following years there was a “boom” of articles focused on fundamental investigations of laser produced plasmas performed over a wide range of laser characteristics (beam power, pulse width, repetition rate etc.). The development of the laser technology and the measurement techniques led to more sophisticated experiments and more comprehensive theoretical models. Exciting results began to arise due to the new means of study, such as visible, ultra-violet and X-ray emission measurements (Ehler and Weissler, 1966; Benavides *et al.*, 2016), coupled with the findings of multiply-charged ions (Archbold and Hughes, 1964) and two- and three-photon emission (Sonnenberg *et al.*, 1964). All these achievements and findings led to the development of new applications that were proposed as alternatives to the already existing ones.

In 1964, Berkowitz and Chupka (1964) proposed for the first time the laser ablation technique as an alternative to fusion, thus arose the idea of laser confinement fusion. Another spectacular application that was born was the Pulsed Laser Deposition (PLD), as a response to the already existing sputtering techniques. Smith and Turner (1965) reported the first representative experiment of PLD. Although the authors experimented on a variety of materials using a ruby laser, the quality of the resulted thin films was secondary to the ones produced by sputtering. Not until the 80's was laser film growth able to compete with the other well established deposition techniques, when Dijkkamp *et al.* (1987) deposited a high quality thin film of YBa₂Cu₃O₇. Since then, the PLD technique has been used to successfully produce thin films with a wide variety of properties, amongst which a series of thin films with high crystallinity (ceramic oxides, nitrides, metallic multilayers) (Eason, 2007; Craciun *et al.*, 1994, 2005; Perriere *et al.*, 2002). The main advantages of PLD are the relatively low costs, with respect to molecular beam epitaxy (MBE) or metal-organic chemical vapor deposition (MOCVD), and the better control over stoichiometry and phase composition, which is very beneficial regarding the growth of complex materials, including high-quality nanomaterials that are impossible to synthesize otherwise. Some of the main successes of the technique can be summed up by the type of complex target resulted (nanowires of Si and Ge (Morales and Lieber, 1998), binary (In₂O₃ (Li *et al.*, 2003), SnO₂ (Liu *et al.*, 2003), ZnO (Yang *et al.*, 2006)) and ternary systems (GaAs_{0.6}P_{0.4}, InAs_{0.5}P_{0.5}, CdS_xSe_{1-x}, indium tin oxide (Savu and Joanni, 2006)), and more complex materials (Eisenhower *et al.*, 2011).

As the thin-film deposition technology flourished, the growing reliability and stability of commercial lasers, particularly Q-switched YAG lasers, improved the uniformity of film growth and the reproducibility of microprobe measurements. Significant progress was made, simultaneously, on

the fundamentals aspects of the deposition process. This was achieved through plume diagnostics and the development of theoretical models. The pulsed laser deposition process is a complex one. This complexity comes also from the correlations between a series of variables like: target composition, laser characteristics as fluence, wavelength or pulse width, background gas species, substrate's physical properties, overall PLD geometry etc. Changing one parameter often shifts the ideal settings for others. The effects of changing a single variable can be identified by keeping all other variables constant, and variables are generally kept constant for simplicity. Due to this network of inter-relationships, the control of the deposition process becomes complicated, as well as the overall understanding of the LPP dynamics and how the properties of the plume can influence the final product. This image can be somehow simplified. Let us observe the deposition process from three different perspectives based on the possible influencing factors. One perspective covers the interactions between the laser beam and the target, governed by the physical properties of the target (reflectivity, thermal/electrical conductivity, heat of vaporization, etc.) and those of the laser beam (wavelength, pulse width, shape, etc.) (Zavestovskaya *et al.*, 2008; Benavides *et al.*, 2016). A second perspective will describe the relationships between the physical properties of the target and the properties of the laser produced plasmas (Williams *et al.*, 2008; Hermann *et al.*, 2012) and the third one the influence of the ejected particles on the properties of the resulted thin film. In order to achieve some knowledge on any of these dependences it is imperative to use well-established investigation techniques (OES, ICCD fast camera imaging, Langmuir probe method, mass spectrometry, etc.) in order to find a unification relationship between all these "variables".

The benefits of the proper use of the investigation techniques further led to the discovery of other spectacular results. Splitting of the plume is one of them and it was first reported by Geohegan's group (Geohegan and Puretzky, 1995, 1996), when investigating the dynamics of LPP in an ambient gas. This group also proposed a theoretical description based on multiple-scattering and hydrodynamic approaches (Leboeuf *et al.*, 1996). The plume splitting has been further confirmed and studied by other groups (Harilal *et al.*, 2002, 2003; Wu *et al.*, 2013). All these results were obtained in typical PLD experimental conditions, *i.e.* fluence in the range of 1 J/cm² and background gas pressure of 1-100 mbar. We emphasize that similar results were also reported for laser ablation in vacuum (background pressure < 10⁻⁵ mbar) and at fluences typically higher than 10 J/cm² (Gurlui *et al.*, 2006, 2008, 2009; Ursu *et al.*, 2009). From a theoretical perspective the plume splitting is seen at the results of two distinct mechanisms for the particle ejection (Kelly and Miotello, 1997 Nica *et al.*, 2009, 2010; Pompilian *et al.*, 2014; Yoo *et al.*, 2000; Ursu *et al.*, 2009): the ions would be ejected on a very short time scale through a Coulomb process in the very intense field left by the electrons laser excitation and detachment, while the

neutrals would come from a subsequent thermal process (phase explosion (Kelly and Miotello, 1998)) which needs more time to establish (Yoo *et al.*, 2000).

Besides the overall dynamics of the plume, looking closely to the individual dynamics of the ejected charged particles, an oscillatory behavior was observed. The first reports of plasma oscillations were published in the 1980's. Borowitz *et al.* (1987) recorded a fast oscillation structure on the target current of about 100 ps period when irradiating with an 100 J, ns laser beam (fluence up to 10^5 J/cm²). The first attempts for the comprehension of this "peculiar" behavior were based on the formation of single or multiple double-layers in the very vicinity of the target. This picture was the main focus to a long series of papers reporting on charge separation in laser-produced plasma, mainly from the 1970 – 1980 (Pearlman and Dahlbacka, 1977; Ludmirsky *et al.*, 1984, 1985). Eliezer (1989) gathered in a very comprehensive manner the state of the art regarding the double and multiple layers in laser-produced plasmas. One of the remarkable results reported are experimental proof with double-layer electric fields of $10^5 - 10^6$ V/cm and widths of 10-100 Debye lengths (Eliezer and Ludmirsky, 1983).

In this short introduction, it was attempted to review a few "firsts". All the results are building blocks as the techniques implemented in the 60's led to the development of new theoretical models and new aspects of the laser-produced plasmas never seen before. The history of laser ablation is full of "firsts": the first optical emission spectroscopy measuring led to the development of the Laser-Induced Breakdown Spectroscopy (LIBS) technique, the first measurements of the ionic energy distribution led to the further development of mass spectrometry or the first picture of the ejected material foreshadowing the development of the ICCD fast camera imaging method. These are pillars on which was built the image that we have today of laser ablation process as a whole. Now we can see the effects of all these great moments in laser ablation history, the rise of fast camera photography paved the way for the plume splitting effects while the probing of the charged particles led to the observation of plasma oscillations.

2. Laser Ablation in Various Temporal Regimes

With the aim of reaching the enthusiastic objectives presented above, we have to understand what can connect the data provided by the typical LPP measurements with the physical properties of the targets. All the available techniques study the ejected particle during expansion (Geohegan, 1992; Lunney *et al.*, 2007; Ursu *et al.*, 2010), thus all the investigations will be performed post laser - target interaction. Henceforth, our main goal becomes to look at the plasma during its expansion and then relate that to the initial properties of the electrons and ions in the target. This aspect becomes essential, as in order to understand the connection between the target and the LPP it is

imperative to assume that the ejected particles and the information that they carry contain the “memory” embedded with the properties of the target. The memory of the ejected particles is mediated through the ablation mechanisms involved with respect to each ablation regime. Since the thesis is focused on the study of laser-produced plasmas in various ablation regimes (ns, ps, fs), we will attempt in the following to present the main mechanisms that manifest at various temporal regimes. In Fig. 1 (Rethfeld *et al.*, 2004) there are presented as examples different processes that take place after the laser energy is absorbed by the lattice of the target. We notice some considerable differences between the ablation regimes used in this thesis. For the fs regime (fs \sim 1 ps) there are mainly non-thermal processes involved which end with the Coulomb explosion as the main ejection mechanism (Shirk and Molian, 1998). For the ps regime, if the pulse width is higher than \sim 10 ps, the thermal mechanisms are becoming predominant, starting with the thermal damage of the lattice (homogeneous melting), if the pulse is shorter, there is defined a transition area between pure non-thermal and thermal effect where Coulomb explosion (Bulgakova *et al.*, 2005) is still the main ablation mechanism and the thermal effects are reduced. In the ns regime, the longer pulse width leads to strong thermal effects followed by the subsequent laser beam absorption by the ejected particles (Mao *et al.*, 2013). Here, mechanisms like Coulomb explosion are secondary to the thermal ones.

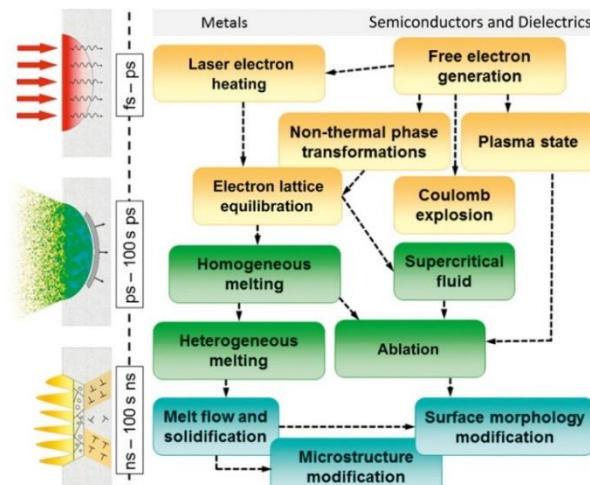


Fig. 1 – Mechanisms involved in various laser ablation regimes (Rethfeld *et al.*, 2004).

The simplest way to describe the ablation process is to divide it into four stages. In the first stage are included all the laser-target interactions such as laser absorption by the target electrons or target heating (Fig. 1). Here we can see the manifestation of the ablation mechanisms. In the second stage, the

particles are ejected from the target and the plume forms. During this stage, in the ns ablation regime and for the ps regime (if the pulse width is higher than 10 ps) the plume absorbs a part of the laser energy (the absorption of the laser radiation is done through single-photon processes (Tokarev *et al.*, 1995), mainly by Inverse Bremsstrahlung (IB) effect (Mao *et al.*, 1996)). Also, at this stage, the laser-plasma interactions are dominant. For the fs and ps (1 - 10 ps) regimes this stage does not exist because the plume expansion occurs after the laser pulse has ended. The third stage occurs after the laser pulse has ended. At this stage, in vacuum conditions, the plume is expanding adiabatically (Doggett and Lunney, 2011). The expansion of the plume differs with respect to the background gas conditions, which leads to the fourth stage that describes the plume dynamics if the ablation takes place in a background gas. After the development of the three stages the plume expansion is dictated by the interactions between the plume particles (ions, atoms, electrons, clusters) and the background gas particles.

Understanding the main processes involved in laser-matter interaction is important for their fundamental relevance and also for comprehending the capabilities and limitations of laser-based applications and technologies. The last ablation stages are used for the diagnosis purposes and where the main “bulk” of information is extracted from the plasma, but before we can delve into studies related to the dynamics of the ejected particles it is essential to emphasize some fundamental aspects of the first stage. Generally, when a laser beam impinges on the material, laser energy is first absorbed by free electrons (Mao *et al.*, 2013). The absorbed energy then propagates through the electron system and is transferred to the lattice (Mao *et al.*, 2013). In literature are identified three characteristic time scales: T_e – the electron cooling time, which is on the order of 1 ps; T_i – the lattice heating time (~ 10 ps); and T_l – the duration of laser pulse.

Let us first consider a general case covering a range of pulse widths from continuous wave (cw) laser to ms pulsed laser, $T_l (\sim \text{ms}) \gg T_i \gg T_e$. The typical time scale is much larger than the electron-lattice energy coupling time, and thus the main processes involved will be the melting and the subsequent ejection of the molten material assisted by the particle gas (Phipps, 2007). This ablation regime is completely described by the classical heat transfer laws which are often used for the modeling of the laser ablation process in the ms regime. Due to the particularities of the ablation mechanism, this regime is often used in applications like laser cutting, which covers a wide range of materials (steel, nonferrous metals, and nonmetals). For shorter ablation regimes ($\sim \text{ns}$) a second case arises: $T_l (\sim \text{ns}) \gg T_i \gg T_e$. In this case, electron absorbed laser energy has enough time to be transferred to the lattice, electrons and lattice can reach thermal equilibrium, and the main energy loss is the heat conduction into the solid target. Therefore, the target is melted, followed by evaporation occurring from the liquid state (Kelly and Miotello, 1998). Usually, the heat

affected zone is smaller than that of the cw laser processing. These properties make ns-laser ablation a powerful tool for technological applications like laser drilling (Lawrence, 2010), grooving, marking, or scribing. Nevertheless, the presence of a melted layer makes precise material removal rather difficult. In this time scale, the typical lasers used are Q-switched solid state lasers, such as the Nd:YAG laser (1024 nm - 266 nm). Another case corresponds to the ultra-fast laser ablation, $T_l \ll T_e \ll T_i$, where T_l is on the femtosecond scale, and laser pulse duration is shorter than the electron cooling time. The electrons in the surface layer undergo cooling by heat diffusion and by heat transfer to the lattice ions. This stage continues for several picoseconds. The picture changes in the case of a semiconductor target that is heated by an ultrashort pulse. The laser energy is deposited into the solid by creating a “bath” of hot electrons and holes (Shirk and Molian, 1998). Hot carriers subsequently transfer energy to the lattice by creating optical and acoustic phonons. In the case of both metals and semiconductors, the thermalization of laser energy in the hot carrier bath takes place within a few femtoseconds (≈ 10 fs), while the typical time-scale for lattice heating falls within the 1 - 10 ps range, where thermal conduction is totally negligible (Leitz *et al.*, 2011).

So far, in the literature the majority of the experimental investigations have been carried by Ti: Sapphire laser systems with variable pulse widths. The same systems are often used for the case of ps laser ablation. There, although the pulse width is much shorter than the typical thermal conduction time (hundreds of ns), the laser pulse duration is of the same order as the hot carriers-lattice relaxation time (few ps).

If we analyze in depth the particularities of the short and ultra-short laser ablation we can differentiate between several ablation regimes. Considering the strong differences between the various temporal regimes (ns, ps, fs), it is of the utmost interest to investigate the laser-produced plasmas in those regimes and try to comprehend how the fundamental mechanism affects the properties of the ablation plasmas. Moreover, the comparative study amongst different targets with different physical properties could allow us to understand the connections that can be made in each specific ablation regime and try to correlate with the physical processes involved in the material removal.

3. Laser Ablation Mechanisms

In the literature (Miller, 1994; Phipps, 2007; Lawrence, 2010; Stafe *et al.*, 2014) the mechanisms are generally divided into two main categories. There are the primary mechanisms that are involved only in the removal of the target material (*Normal Vaporization, Normal Boiling, Phase Explosion* and *Coulomb Explosion*) and the secondary mechanisms meant to describe the behavior of the expelled particles after the interaction between the laser beam and the target

surface took place (*Knudsen-Layer Processes, Effusion-Like Release and Normal Outflow*). A better way we can differentiate between the ablation mechanisms is by the type of processes involved. Using these criteria, we can attribute mechanisms for each ablation regime. Thus, we find thermal (Normal Vaporization, Normal Boiling and Phase Explosion) and electrical (Electronic Processes, Coulomb Explosion) mechanisms. For the nanosecond or longer pulse lasers the thermal mechanisms are dominant and for the picosecond or shorter the electrical ones are dominant. Also, for the ultrafast lasers the interaction time between the laser beam and the target is shorter and as a result the mechanisms involved in the removal of the target particles can be different from the ones involved in the nanosecond laser ablation.

3.1. Normal Vaporization and Normal Boiling

Normal vaporization is a term which describes a group of processes having in common a thermal origin. This mechanism does not have a dependence on the laser fluence or pulse length, thus the main dependence is on the properties of the target. The term “thermal” is not accurate enough to describe this process, as it was reported by (Mele *et al.*, 1997), due to the fact that the temperature (which is usually a measure of a system at equilibrium) is transient, they suggested that a more accurate term would be “thermal spike”. As a result of laser-matter interactions, the atoms, electron, ions, etc. are ejected from the outer layer of the surface. Due to the short interaction time vapor bubbles do not form at the surface, nor from layer beneath the surface. In this scenario, the particle flux emitted can be described by the Hertz-Knudsen equation:

$$\text{Particle flux} = \alpha(p_{sv} - p_v)(2\pi mk_B T)^{-\frac{1}{2}} (\text{particles} / \text{s cm}^2) \quad (1)$$

where α is the vaporization coefficient (Anisimov *et al.*, 1974), p_{sv} – the saturated vapor pressure, p_v – the vapor pressure, m – the particle mass, T – the surface temperature and k_B – the Boltzmann constant. By multiplying Eq. (1) by m / ρ ($\equiv \lambda^3$), where ρ is the mass density and λ is the length of the atomic bond, then it will define the velocity of the surface recession in a 1-D situation:

$$\left. \frac{\partial x}{\partial t} \right|_{x=0} = \alpha(p_{sv} - p_v)(2\pi mk_B T)^{-\frac{1}{2}} \lambda^3 (\text{cm} / \text{s}) \quad (2)$$

$$= \alpha \left[p_b e^{\frac{\Delta H_v m}{k_B} \left(\frac{1}{T_b} - \frac{1}{T} \right)} - p_v \right] (2\pi mk_B T)^{-1/2} \lambda^3 \quad (3)$$

where ΔH_v is the heat of vaporization, assuming there is no re-condensation (Yoo *et al.*, 2000), p_b is the boiling pressure and T_b the boiling temperature. A

second type of thermal spike often reported in the literature requires a longer pulse length, long enough for the heterogeneous nucleation of the vapor bubble (Dell’Aglia *et al.*, 2015) to occur. If p_v is higher than p_b the “normal boiling” will occur. However, the density of nucleation sites is rather low (Yoo *et al.*, 2000), this means that although the necessary conditions are met, the main ablation mechanism still remains normal vaporization.

3.2. Phase Explosion

In order for the phase explosion to manifest itself, it requires high laser fluences and relatively short pulse widths (ns, ps, fs) (Schittenhelm *et al.*, 1996). In literature are reported some specific thresholds for this ablation mechanism, related to the laser beam properties and the physical properties of the target (mainly the laser wavelength and the binding energy of the target lattice ions) (Russo *et al.*, 2000; Yoo *et al.*, 2000). The main result that can be quantified using phase explosion as an ablation mechanism is the overall quantity of the ablated mass per pulse. From an experimental point of view the quantity of ablated mass can be also correlated to the depth of the crater made by the laser beam (Fig. 2).

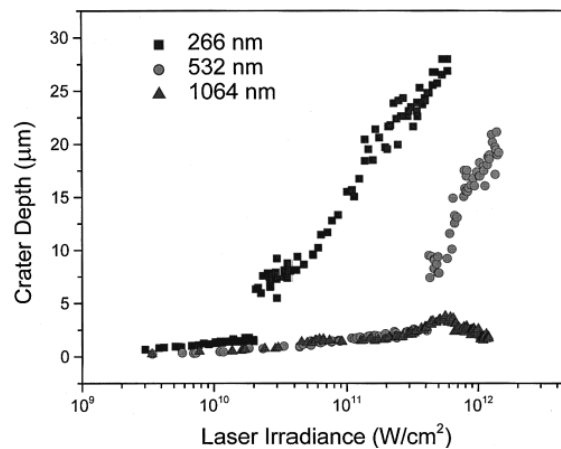


Fig. 2 – Dependence of the crater depth on the incident laser wavelength and irradiance (Schittenhelm *et al.*, 1996).

If the laser beam fluence is high enough, above the threshold, the surface will reach a temperature of $\sim 0.9 \cdot T_c$ (T_c is the thermodynamic critical temperature). Close to the thermodynamic critical temperature the vapor nucleation rate raises (Martynyuk, 1977), because the necessity of the nuclei formation is no longer a kinetic obstacle. It was shown that the formation rate of nuclei has a big variation from $10^{-25} \text{ cm}^{-3} \text{ s}^{-1}$ to $10^{25} \text{ cm}^{-3} \text{ s}^{-1}$ when the temperature

increases from $0.88 T/T_c$ to $0.92 T/T_c$ (Yoo *et al.*, 2000). Also, due to the high temperature, the nucleation of the homogenous vapor bubbles occurs and these vapor bubbles reach a critical size. The size of the bubbles is characterized by the critical radius, with the bubbles having a lower radius most probably collapsing. Generally speaking, the target changes its state from superheated liquid to mixture of liquid droplets and vapors. In the end, the bubbles explode and the particles and the clusters are ejected. The presence of the phase explosion is followed by an increase in the quantity of mass removed, as it was reported by Yoo *et al.* (2000). The increase in the mass removed will lead to an increase of the crater (Yoo *et al.*, 2000) created by the laser pulse as it is shown in Fig. 3.

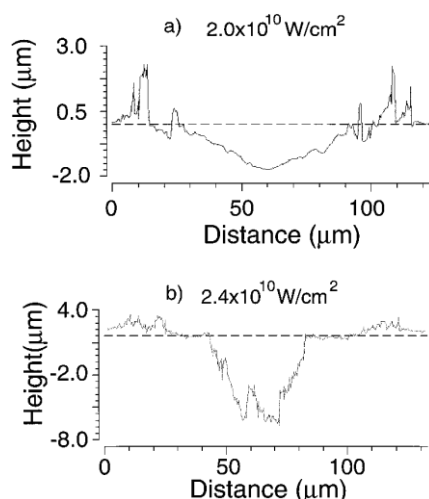


Fig. 3 – Cross-sectional images of the crater for: *a* – laser irradiance slightly below the phase explosion threshold (20 GW/cm^2) and *b* – laser irradiance slightly above the threshold (24 GW/cm^2) (Schittenhelm *et al.*, 1996).

Further studies have shown also that the ejected vapors and the liquid droplets are separated in time. Therefore, due to the difference in their mass, the vapors are reported to be detectable at $t < 500 \text{ ns}$, while the droplets at $t > 25 \text{ } \mu\text{s}$ (Schittenhelm *et al.*, 1996; Kelly and Miotello, 1997; Yoo *et al.*, 2000). These conclusions were further used to understand results related to the structure and overall dynamics of the ejected cloud obtained by ICCD fast camera imaging and Langmuir probe measurements (Harilal *et al.*, 2002; Ursu *et al.*, 2009; Irimiciuc *et al.*, 2014, 2017; Focșa *et al.*, 2017).

3.3. Coulomb Explosion

The *Coulomb explosion* is one of the electrostatic mechanisms of the laser ablation (Bulgakova *et al.*, 2005). This mechanism has been discussed in

many papers over the last years (Jiang and Tsai, 2003; Dachraoui *et al.*, 2006; Werner and Hashimoto, 2011; Lin *et al.*, 2012; Focșa *et al.*, 2017). Coulomb explosion plays an important role in different applications such as surface nanostructuring (Rapp *et al.*, 2016) or nanoparticle formation (De Giacomo *et al.*, 2013). Coulomb explosion has been observed first on dielectric materials, while for semiconductors and metals the subject remained controversial (Gamaly *et al.*, 2002). It was however proven that for higher fluences of the laser beam, the generated electric field can be high enough for the disintegration of the surface even for semiconductors and metals (Bulgakova *et al.*, 2004).

One of the important results was the reporting of the energetic ions of several species having the same momenta but different energies (Stoian *et al.*, 2000). Other reports (Ursu *et al.*, 2009, 2010; Pompilian *et al.*, 2013; Irimiciuc *et al.*, 2017; Wellershoff *et al.*, 1999) based on investigation of the overall dynamics of the plume and individual kinetics of the ejected particles through optical methods revealed that doubly-charged ions had the velocities almost twice as high as the single-charged ions. The difference indicates that the ions are accelerated in the same electric field. The electric field is generated by intensive electron photoemission and by the separation between the fast escaping electrons and the ions left on the surface (or in the plume, but behind the electrons). Usually the repulsive force between ions is higher than the binding energy, which results in the disintegration of the surface (Fig. 4).

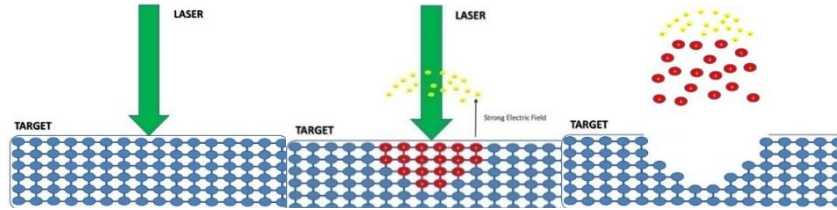


Fig. 4 – The stages of the Coulomb Explosion.

If the electric field, generated by photoemission, is higher than the atomic bonding energy, the density of the electrostatic energy per atom has to exceed the value of the sublimation energy per atom. For an ultra-short laser (fs, ps), where the thermal mechanisms do not play an important part, the threshold electric field can be approximated as:

$$E_{c_f}|_{x=0} = \sqrt{\frac{2\Lambda n_0}{\epsilon\epsilon_0}} \quad (4)$$

where Λ (kJ/mol) is the sublimation energy per atom, n_0 (cm^{-3}) is the lattice density, and ϵ is the dielectric permittivity. For longer pulses (ns, ps) it has to be taken into account the heating of the lattice. Due to the heating, the vibrational

energy of the atoms increases and the probability of the atoms to escape from the target due to thermal effects increases. That being said, Eq. (4) further becomes:

$$E_{C_n} \Big|_{x=0} = \sqrt{\frac{2(\Lambda - 3k_B T_s)n_0}{\epsilon\epsilon_0}} \quad (5)$$

4. Conclusions and Perspective

The complexity of all the processes involved lead to the implementation of complicated investigation techniques that often only capture a particular facet of the laser produced plasma. The optical diagnostics only captures information about the excited states present in the plasma, the electrical ones follow the dynamics of charged particles, while techniques involving mass spectrometry offer information about the molecules and clusters formed during the ablation process. The solution to have a more complete image of the laser produced plasmas, is the use of complimentary method in a simultaneous manner.

Also, a good alternative to the experimental approach is the use of appropriate theoretical model that would ideally, cover all the fundamental processes and ablation mechanisms. Since Coulomb Explosion and Phase Explosion do manifest themselves at different temporal scale, preferably the theoretical model needs incorporate be a multi-scale, multi-physics type approach. All the requirements are covered by the fractal hydrodynamic model proposed by our group about ten years ago, that recently showed how the differences in the fundamental mechanism involved in various ablation regimes reflect the fractalization of the system. Such a mathematical approach can be used to study the dynamic of similar systems that can be assimilated to a fractal fluid like discharge plasmas, polymers, blood or other complex polymers (Agop *et al.*, 2009, 2010; Anisimov and Rakhmatulina, 1973).

REFERENCES

- Agop M., Nica P.E., Gurlui S., Focșa C., Păun V.P., Colotin M., *Implications of an Extended Fractal Hydrodynamic Model*, Eur. Phys. J. D, **56**, 3,405-419 (2009).
 Agop M., Nica P., Gurlui S., Focșa C., *Fractal Hydrodynamic Model of High-Fluence Laser Ablation Plasma Expansion*, AIP Conf. Proc., **1728**, 64, 482-491 (2010).
 Anisimov S.I., Kapeliovich B.L., Perel'man T.L., Landau L.D., *Electron Emission from Metal Surfaces Exposed to Ultrashort Laser Pulses*, Sov. Phys. JETP, **39**, 2, 375-377 (1974).
 Anisimov S.I., Rakhmatulina K.H., *The Dynamics of the Expansion of a Vapor when Evaporated into a Vacuum*, Zh. Eksp. Teor. Fiz., **37**, 3, 441-444 (1973).
 Archbold E., Hughes T.P., *Electron Temperature in a Laser-Heated Plasma*, Nature, **204**, 4959, 670 (1964).

- Askar'yan G.A., Moroz E.M., *Pressure on Evaporation of Matter in a Radiation Beam*, Sov. Phys. JETP, **13**, 1638-1639 (1963).
- Benavides O., de la Cruz L., Meja E.B., Ruz Hernandez J.A., Flores Gil A., *Laser Wavelength Effect on Nanosecond Laser Light Reflection in Ablation of Metals*, Laser Phys., **26**, 12, 126101 (2016).
- Berkowitz J., Chupka W.A., *Mass Spectrometric Study of Vapor Ejected from Graphite and Other Solids by Focused Laser Beams*, J. Chem. Phys., **40**, 9, 2735-2736 (1964).
- Borowitz J.L., Eliezer S., Gazit Y., Givon M., Jackel S., Ludmirsky A., Salzmann D., Yarkoni E., Zigler A., Arad B., *Temporally Resolved Target Potential Measurements in Laser-Target Interactions*, J. Phys. D. Appl. Phys., **20**, 2, 210-214 (1987).
- Bulgakova N.M., Stoian R., Rosenfeld A., Hertel I.V., Campbell E.E.B., *Electronic Transport and Consequences for Material Removal in Ultrafast Pulsed Laser Ablation of Materials*, Phys. Rev. B, **69**, 5, 54102 (2004).
- Bulgakova N.M., Stoian R., Rosenfeld A., Hertel I.V., Marine W., Campbell E.E.B., *A General Continuum Approach to Describe Fast Electronic Transport in Pulsed Laser Irradiated Materials: The Problem of Coulomb Explosion*, Appl. Phys. A Mater. Sci. Process., **81**, 2, 345-356 (2005).
- Crăciun V., Elders J., Gardeniers J.G.E., Boyd I.W., *Characteristics of High Quality ZnO Thin Films Deposited by Pulsed Laser Deposition*, Appl. Phys. Lett., **65**, 23, 2963-2965 (1994).
- Crăciun V., Crăciun D., *Pulsed Laser Deposition of Crystalline LaB₆ Thin Films*, Appl. Surf. Sci., **247**, 1-4, 384-389 (2005).
- Dachraoui H., Husinsky W., Betz G., *Ultra-Short Laser Ablation of Metals and Semiconductors: Evidence of Ultra-Fast Coulomb Explosion*, Appl. Phys. A Mater. Sci. Process., **83**, 2, 333-336 (2006).
- Dell'Aglio M., Gaudiuso R., De Pascale O., De Giacomo A., *Mechanisms and Processes of Pulsed Laser Ablation in Liquids During Nanoparticle Production*, Appl. Surf. Sci., **348**, 4-9 (2015).
- De Giacomo A., Gaudiuso R., Koral C., Dell'Aglio M., De Pascale O., *Nanoparticle-Enhanced Laser-Induced Breakdown Spectroscopy of Metallic Samples*, Anal. Chem., **85**, 21, 10180-10187 (2013).
- Doggett B., Lunney J.G., *Expansion Dynamics of Laser Produced Plasma*, J. Appl. Phys., **109**, 9, 093304 (2011).
- Dijkkamp D., Venkatesan T., Wu X.D., Shaheen S.A., Jisrawi N., Min-Lee Y.H., McLean W.L., *Preparation of Y-Ba-Cu Oxide Superconductor Thin Films Using Pulsed Laser Evaporation from High T_c Bulk Material*, Appl. Phys. Lett., **51**, 8, 619-621 (1987).
- Eason R., *Pulsed Laser Deposition of thin Films: Applications-Led Growth of Functional Materials*, Wiley-Interscience, New Jersey (2007).
- Ehler A.W., Weissler G.L., *Vacuum Ultraviolet Radiation from Plasmas Formed by a Laser on Metal Surfaces*, Appl. Phys. Lett., **8**, 4, 89-91 (1966).
- Eisenhawer B., Zhang D., Clavel R., Berger A., Michler J., Christiansen S., *Growth of Doped Silicon Nanowires by Pulsed Laser Deposition and Their Analysis by Electron Beam Induced Current Imaging*, Nanotechnology, **22**, 7, 75706 (2011).
- Eliezer S., *Double Layers in Laser-Produced Plasmas*, Phys. Rep., **172**, 6, 339-407 (1989).

- Eliezer S., Ludmirsky A., *Double Layer (DL) Formation in Laser-Produced Plasma*, Laser Part. Beams, **1**, 3, 251-269 (1983).
- Focșa C., Gurlui S., Nica P., Agop M., Ziskind M., *Plume Splitting and Oscillatory Behavior in Transient Plasmas Generated by High-Fluence Laser Ablation in Vacuum*, Appl. Surf. Sci., **424**, 3, 299-309 (2017).
- Gamaly E.G., Rode A.V., Luther-Davies B., Tikhonchuk V.T., *Ablation of Solids by Femtosecond Lasers: Ablation Mechanism and Ablation Thresholds for Metals and Dielectrics*, Phys. Plasmas, **9**, 3, 949-957 (2002).
- Geohegan D.B., *Fast-Iccd Photography and Gated Photon Counting Measurements of Blackbody Emission from Particulates Generated in the KrF-Laser Ablation of BN and YBCO*, MRS Proc., **285**, 27-32 (1992).
- Geohegan D.B., Poretzky A.A., *Laser Ablation Plume Thermalization Dynamics in Background Gases: Combined Imaging, Optical Absorption and Emission Spectroscopy, and Ion Probe Measurements*, Appl. Surf. Sci., **96-98**, 131-138 (1996).
- Geohegan D.B., Poretzky A.A., *Dynamics of Laser Ablation Plume Penetration Through Low Pressure Background Gases*, Appl. Phys. Lett., **67**, 2, 197-199 (1995).
- Gurlui S., Sanduloviciu M., Strat M., Strat G., Miheșan C., Ziskind M., Focșa C., *Dynamic Space Charge Structures in High Fluence Laser Ablation Plumes*, J. Optoelectron. Adv. Mater., **8**, 1, 148-151 (2006).
- Gurlui S., Agop M., Nica P., Ziskind M., Focșa C., *Experimental and Theoretical Investigations of a Laser Produced Aluminum Plasma*, Phys. Rev. E, **78**, 026405 (2008).
- Gurlui S., Sanduloviciu M., Miheșan C., Ziskind M., Focșa C., *Periodic Phenomena in Laser-Ablation Plasma Plumes: A Self-Organization Scenario*, AIP Conf. Proc., **812**, 1, 279-282 (2009).
- Harilal S.S., Bindhu C.V., Tillack M.S., Najmabadi F., Gaeris A.C., *Plume Splitting and Sharpening in Laser-Produced Aluminium Plasma*, J. Phys. D. Appl. Phys., **35**, 22, 2935-2938 (2002).
- Hermann J., Mercadier L., Axente E., Noël S., *Properties of Plasmas Produced by Short Double Pulse Laser Ablation of Metals*, J. Phys. Conf. Ser., **399**, 12006 (2012).
- Honig R.E., Woolston J.R., *Laser-Induced Emission of Electrons, Ions, and Neutral Atoms From Solid Surfaces*, Appl. Phys. Lett., **2**, 138 (1963).
- Howe J.A., *Observations on the Maser Induced Graphite Jet*, J. Chem. Phys., **39**, 5, 1362-1363 (1963).
- Irimiciuc S., Boidin R., Bulai G., Gurlui S., Nemeș, Nazabal V., Focșa C., *Laser Ablation of $(GeSe_2)_{100-x}(Sb_2Se_3)_x$ Chalcogenide P. Glasses: Influence of the Target Composition on the Plasma Plume Dynamics*, Appl. Surf. Sci., **418(B)**, 594-600 (2017).
- Irimiciuc S.A., Mihăilă I., Agop M., *Experimental and Theoretical Aspects of a Laser Produced Plasma*, Phys. Plasmas, **21**, 9, 093509 (2014).
- Jiang L., Tsai H.L., *Femtosecond Lasers Ablation: Challenges and Opportunities*, Aerosp. Eng., **1**, 1, 51-53 (2003).
- Kelly R., Miotello A., *On the Mechanisms of Target Modification by Ion Beams and Laser Pulses*, Nucl. Instrum. Meth. B, **122**, 3, 374-400 (1997).
- Kelly R., Miotello A., *On the Role of Thermal Processes in Sputtering and Composition Changes Due to Ions or Laser Pulses*, Nucl. Instrum. Meth. B, **141**, 1-4, 49-60 (1998).

- Lawrence J., *Advances in Laser Materials Processing: Technology, Research and Applications*, Woodhead Publishing, Cambridge (2010).
- Leboeuf J.N., Chen K.R., Donato J.M., Geohegan D.B., Liu C.L., Poretzky A.A., Wood R.F., *Modeling of Dynamical Processes in Laser Ablation*, Appl. Surf. Sci., **96–98**, 14-23 (1996).
- Leitz K.-H., Redlingshöfer B., Reg Y., Otto A., Schmidt M., *Metal Ablation with Short and Ultrashort Laser Pulses*, Phys. Proc., **12**, 230-238 (2011).
- Li C., Zhang D., Han S., Liu X., Tang T., Zhou C., *Diameter-Controlled Growth of Single-Crystalline In₂O₃ Nanowires and Their Electronic Properties*, Adv. Mater., **15**, 2, 143-146 (2003).
- Lichtman D., Ready J.F., *Laser Beam Induced Electron Emission*, Phys. Rev. Lett., **10**, 8, 342-345 (1963).
- Lin X., Chen H., Jiang S., Zhang C., *A Coulomb Explosion Theoretical Model of Femtosecond Laser Ablation Materials*, Sci. China Technol. Sc., **55**, 3, 694-701 (2012).
- Liu Z., Zhang D., Han S., Li C., Tang T., Jin W., Liu X., Lei B., Zhou C., *Laser Ablation Synthesis and Electron Transport Studies of Tin Oxide Nanowires*, Adv. Mater., **15**, 20, 1754-1757 (2003).
- Ludmirsky A., Givon M., Eliezer S., Gazit Y., Jackel S., Krumbein A., Szichman H., *Electro-Optical Measurements of High Potentials in Laser Produced Plasmas with Fast Time Resolution*, Laser Part. Beams, **2**, 2, 245-250 (1984).
- Ludmirsky A., Eliezer S., Arad B., Borowitz A., Gazit Y., Jackel S., Krumbein A.D., Salzmann D., Szichman H., *Experimental Evidence of Charge Separation (Double Layer) in Laser-Produced Plasmas*, IEEE Trans. Plasma Sci., **13**, 3, 132-134 (1985).
- Lunney J.G., Doggett B., Kaufman Y., *Langmuir Probe Diagnosis of Laser Ablation Plasmas*, J. Phys. Conf. Ser., **59**, 470-474 (2007).
- Mao X., Chan W.T., Caetano M., Shannon M.A., Russo R.E., *Preferential Vaporization and Plasma Shielding During Nano-Second Laser Ablation*, Appl. Surf. Sci., **96–98**, 126-130 (1996).
- Mao X., Yoo J., Gonzalez J.J., Russo R.E., *Femtosecond vs. Nanosecond Laser Pulse Duration for Laser Ablation Chemical Analysis*, Spectroscopy, **28**, 6162-6177 (2013).
- Martynyuk M.M., *Phase Explosion of a Metastable Fluid*, Combust. Explo. Shock+, **13**, 2, 178-191 (1977).
- Mele A., Giardini A., Kelly R., Flamini C., Orlando S., *Laser Ablation of Metals: Analysis of Surface-Heating and Plume-Expansion Experiments*, Appl. Surf. Sci., **109–110**, 584-590 (1997).
- Miller C.J., *Laser Ablation: Principles and Applications*, Springer, Berlin (1994).
- Morales A.M., Lieber C.M., *A Laser Ablation Method for the Synthesis of Crystalline Semiconductor Nanowires*, Science, **279**, 5348, 208-211 (1998).
- Neuman F., *Momentum Transfer and Cratering Effects Produced by Giant Laser Pulses*, Appl. Phys. Lett., **4**, 9, 167-169 (1964).
- Nica P., Vizureanu P., Agop M., Gurlui S., Focșa C., Fornă N., Ioannou P.D., Borsos Z., *Experimental and Theoretical Aspects of Aluminum Expanding Laser Plasma*, Jpn. J. Appl. Phys., **48**, 1-7 (2009).

- Nica P., Agop M., Gurlui S., Focșa C., *Oscillatory Langmuir Probe Ion Current in Laser-Produced Plasma Expansion*, Europhys. Lett., **89**, 6, 65001 (2010).
- Pearlman J.S., Dahlbacka G.H., *Charge Separation and Target Voltages in Laser-Produced Plasmas*, Appl. Phys. Lett., **31**, 7, 414-417 (1977).
- Perrière J., Millon E., Seiler W., Boulmer-Leborgne C., Crăciun V., Albert O., Louergue J.C., Etchepare J., *Comparison Between ZnO Films Grown by Femtosecond and Nanosecond Laser Ablation*, J. Appl. Phys., **91**, 2, 690-696 (2002).
- Phipps C.R., *Laser Ablation and its Applications*, Springer US, Boston (2007).
- Pompilian O.G., Gurlui S., Nemeș P., Nazabal V., Ziskind M., Focșa C., *Plasma Diagnostics in Pulsed Laser Deposition of GaLaS Chalcogenides*, Appl. Surf. Sci., **278**, 352-356 (2013).
- Pompilian O.G., Dascălu G., Mihăilă I., Gurlui S., Olivier M., Nemeș P., Nazabal V., Cimpoeșu N., Focșa C., *Pulsed Laser Deposition of Rare-Earth-Doped Gallium Lanthanum Sulphide Chalcogenide Glass Thin Films*, Appl. Phys. A-Mater., **117**, 1, 197-205 (2014).
- Rapp S., Schmidt M., Huber H.P., *Selective Femtosecond Laser Structuring of Dielectric Thin Films with Different Band Gaps: A Time-Resolved Study of Ablation Mechanisms*, Appl. Phys. A, **122**, 12, 1035 (2016).
- Ready J.F., *Development of Plume of Material Vaporized by Giant-Pulse Laser*, Appl. Phys. Lett., **3**, 1, 11-13 (1963).
- Rethfeld B., Sokolowski-Tinten K., von der Linde D., Anisimov S.I., *Timescales in the Response of Materials to Femtosecond Laser Excitation*, Appl. Phys. A, **79**, 4-6, 767-769 (2004).
- Russo R.E., Mao X.L., Borisov O.V., Liu H., *Influence of Wavelength on Fractionation in Laser Ablation ICP-MS*, J. Anal. Atom. Spectrom., **15**, 9, 1115-1120 (2000).
- Savu R., Joanni E., *Low-Temperature, Self-Nucleated Growth of Indium-Tin Oxide Nanostructures by Pulsed Laser Deposition on Amorphous Substrates*, Scripta Mater., **55**, 11, 979-981 (2006).
- Schittenhelm H., Callies G., Berger P., Hügel H., *Investigations of Extinction Coefficients During Excimer Laser Ablation and Their Interpretation in Terms of Rayleigh Scattering*, J. Phys. D. Appl. Phys., **29**, 6, 1564-1575 (1996).
- Shirk M.D., Molian P.A., *A Review of Ultrashort Pulsed Laser Ablation of Materials*, J. Laser Appl., **10**, 1, 18-28 (1998).
- Smith H.M., Turner A.F., *Vacuum Deposited Thin Films Using a Ruby Laser*, Appl. Opt., **4**, 1, 147 (1965).
- Sonnenberg H., Heffner H., Spicer W., *Two-Photon Photoelectric Effect in Cs₃Sb₁*, Appl. Phys. Lett., **5**, 5, 95-96 (1964).
- Stafe M., Marcu A., Puscas N.N., *Pulsed Laser Ablation of Solids: Basics, Theory and Applications*, Springer-Verlag, Berlin (2014).
- Stoian R., Ashkenasi D., Rosenfeld A., Campbell E.E.B., *Coulomb Explosion in Ultrashort Pulsed Laser Ablation of Al₂O₃*, Phys. Rev. B, **62**, 19, 13167-13173 (2000).
- Tokarev V.N., Lunney J.G., Marine W., Sentis M., *Analytical Thermal Model of Ultraviolet Laser Ablation with Single-Photon Absorption in the Plume*, J. Appl. Phys., **78**, 2, 1241-1246 (1995).
- Ursu C., Gurlui S., Focșa C., Popa G., *Space- and Time-Resolved Optical Diagnosis for the Study of Laser Ablation Plasma Dynamics*, Nucl. Instrum. Meth. B, **267**, 2, 446-450 (2009).

- Ursu C., Pompilian O.G., Gurlui S., Nica P., Agop M., Dudeck M., Focșa C., *Al₂O₃ Ceramics Under High-Fluence Irradiation: Plasma Plume Dynamics Through Space- and Time-Resolved Optical Emission Spectroscopy*, Appl. Phys. A, **101**, 1, 153-159 (2010).
- Wellershoff S.-S., Hohlfeld J., Güdde J., Matthias E., *The Role of Electron-Phonon Coupling in Femtosecond Laser Damage of Metals*, Appl. Phys. A-Mater., **69**, S1, S99-S107 (1999).
- Werner D., Hashimoto S., *Improved Working Model for Interpreting the Excitation Wavelength- and Fluence-Dependent Response in Pulsed Laser-Induced Size Reduction of Aqueous Gold Nanoparticles*, J. Phys. Chem.C, **115**, 12, 5063-5072 (2011).
- Williams G.O., O'Connor G.M., Mannion P.T., Glynn T.J., *Langmuir Probe Investigation of Surface Contamination Effects on Metals During Femtosecond Laser Ablation*, Appl. Surf. Sci., **254**, 5921-5926 (2008).
- Wu J., Li X., Wei W., Jia S., Qiu A., *Understanding Plume Splitting of Laser Ablated Plasma: A View from ion Distribution Dynamics*, Phys. Plasmas, **20**, 11, 113512 (2013).
- Yang R., Chueh Yu.L., Morber J.R., Snyder R., Chou L.-J., Wang Z.L., *Single-Crystalline Branched Zinc Phosphide Nanostructures: Synthesis, Properties and Optoelectronic Devices*, Nano.-Micro. Lett., **7**, 2, 269-275 (2006).
- Yoo J.H., Jeong S.H., Mao X.L., Greif R., Russo R.E., *Evidence for Phase-Explosion and Generation of Large Particles During High Power Nanosecond Laser Ablation of Silicon*, Appl. Phys. Lett., **76**, 6, 783-785 (2000).
- Zavestovskaya I.N., Glazov O.A., Demchenko N.N., *Threshold Characteristics of Ultrashort Laser Pulse Ablation of Metals*, Proc. 3rd Int. Conf. Front. Plasma Phys. Technol., **3**, 10-18 (2008).
- Zhvayvi S.P., Ivlev G.D., *Influence of the Initial Temperature of Silicon on Crystallization of a Layer Melted by Nanosecond Laser Heating*, J. Eng. Phys. Thermophys., **69**, 5, 608-611 (1996).

ABLAȚIA LASER: STADIU ACTUAL ȘI PERSPECTIVE

(Rezumat)

În această lucrare se prezintă o trecere în revistă a principalelor descoperiri și dezvoltări ce au avut loc în ultimii zeci de ani pe domeniul ablației laser. Accentul este pus pe tehnologiile dezvoltate pentru a evidenția diversele comportamente ale plasmei și principalele rezultate raportate în literatură. Observațiile experimentale cât și abordările teoretice sunt discutate în raport cu procesele fundamentale ce duc la îndepărtarea materialului țintei prin ablație laser. Mecanismele fundamentale sunt discutate amplu pentru diverse regimuri temporale de ablație și se prezintă cele două mari categorii de mecanisme: electrostatice (explozia Coulomb) și termice (explozia de fază). Înțelegerea acestor aspecte fundamentale duce la posibile dezvoltări tehnologice cât și a modelelor matematice ce iau în considerare gradul de complexitate ridicat al acestui proces.

BULETINUL INSTITUTULUI POLITEHNIC DIN IAȘI
Publicat de
Universitatea Tehnică „Gheorghe Asachi” din Iași
Volumul 63 (67), Numărul 4, 2017
Secția
MATEMATICĂ. MECANICĂ TEORETICĂ. FIZICĂ

EMBEDDING THEORY IN COMPLEX SYSTEMS

BY

IRINEL CASIAN BOTEZ^{1,*}, IULIANA OPREA² and MARICEL AGOP³

¹“Gheorghe Asachi” Technical University of Iași,
Faculty of Electronics, Telecommunication and Information Technology

²Colorado State University, U.S.A

³“Gheorghe Asachi” Technical University of Iași,
Department of Physics

Received: November 18, 2017

Accepted for publication: December 12, 2017

Abstract. In this article we present an introduction in the embedding theory, which is a mean to mathematically describe the very irregular physical processes occurring in complex systems, such as fluid turbulence or those processes occurred at the nanoscale.

Keywords: non-differentiable physical processes; Lagrangean physical systems.

1. Introduction

The modeling in physics is based on differential models that use ordinary differential equations and/or partial differential equations. The use of these equations does not allow, however, the modeling of sufficiently irregular dynamic behavior. In most of the real physical problems, some of the phenomena escape from modeling, either because we do not know them (and nothing tells us that those that escape have to be modeled by differentiable patterns), or because we do not know how to model them (*i.e.* the variation of the sun's flattening over time, which should be taken into account in the

*Corresponding author; *e-mail*: irinel_casian@yahoo.com

evolution studies of the solar system over long periods of time). Therefore, current physical patterns are *regular traces* of more complex dynamics, which are not directly accessible to us.

The embedding theory of dynamical systems consists of trying to model more general dynamics from which, the regular dynamics described by partial differential equations, derive.

2. Embedding Theory

The strategy of embedding theory was first outlined in (Cresson, 2003). In order to describe this strategy, a series of notions should be introduced. It is embedded a functional $L(x, dx/dt)$, defined for $x \in C^1(\mathbb{R})$ in $C^0(\mathbb{R})$ and an operator D that satisfies the following constants: i) D is defined on $C^0(\mathbb{R})$, ii) $D = d/dt$ on $C^1(\mathbb{R})$.

Noting with P the extended functional L , after the embedding, to $C^0(\mathbb{R})$ we have the following diagram:

$$\begin{array}{ccc} L(x, dx/dt) & \xrightarrow{LAP} & EL \\ \downarrow P & & \downarrow P \\ L(X, DX) & \xrightarrow{?} & P(EL) \end{array} \quad (1)$$

where LAP is the least action principle, (EL) is the Euler-Lagrange classical equation associated with L and $(?)$ is, for the time being, an unknown principle of the minimum action, which have to be defined case by case. The ignorance results from the lack of a correct definition of extreme notion and variation for the extended function. The extreme will have to be searched so as to make the diagram (1) switchable. The study of the existence of such an extreme is called *the coherence theorem* in embedding theory. The central point remains the extension of the classical derivative to a more general functional space.

By this extension of the notion of derivative we can reach two distinct theories.

In one case, the initial EL equation is present in the extended EL equation, $P(EL)$. The new derivative is reduced to the classical derivative when returning to classical processes. For example, in the case of stochastic embedding, the new operator reduces to the classical derivative when returning to differentiable deterministic processes (Cresson and Darses, 2007). The terminology used in this case is even embedding theory. The scheme used in this case is the following:

– we extend classical derivatives to a functional space \mathbf{F} and defines an application $p : C^0 \rightarrow \mathbf{F}$ that associates each continuous

function (differentiable or not) with a functional which has the meaning of extended derivative.

– we extend the ordinary differential equations or the partial differential equations using the functional as an extended derivative.

Therefore, the original equation will recover from the extended equation by restricting the functional space to $p(C^k)$, k depending on the order of the original equation. The typical example in this case is *fractional embedding* (Cresson, 2007).

In the second case, an additional parameter, h , is used, and the extended operator, D_h is reduced to the classical derivative only when. In this case, the original EL equation is not contained in the extended equation $P(EL)$; however, we have a continuous deformation of the $P(EL)$ equation, which depends on. In this case, the terminology of *deformation theory* is used. The scheme used in this case is the following:

– we define a family of functional $\{\mathbf{F}\}$ which depend of one or more parameters. For comprehension, consider a single parameter and therefore the functional family dependent on this parameter $\{\mathbf{F}\}_{p_0}$.

– we define an operator D_{p_0} in such a way as when $C^1 \subset \{\mathbf{F}\}_{p_0}$ we have $D_{p_0}(x) = dx/dt$ for $x \in C^1$.

It is obvious that from a deformation we can hardly get information about the initial equation. Asymptotic solutions should be sought for $p_0 \rightarrow 0$.

An example of this is the *scale calculation*. In this case, it is desired to capture the type of regularity of the graph of a function (trajectories) starting from a family of approximations having the following behaviour: if $\varepsilon \neq 0$, then the approximation is a differentiable function, and if $\varepsilon = 0$, then we obtain the original, non-differentiable function. Here ε is the scale resolution. In this approach, the notion of minimal resolution appears to be necessary, but its definition still requires discussions, and there is no intrinsic definition of this notion because this is about choosing a constant, which in practice, would preserve the role of precision, what has physical meaning, but not mathematical one.

3. Conclusions

Linear or nonlinear Schrodinger's equation can be obtained as a result of a principle of the minimal action formulated in one of two cases (embedding or deformation). These results suggest the following.

i) Any natural equation with partial derivatives could be obtained as a result of a minimum action principle. As natural we understand partial

differential equations well known in physics, such as, for example, the Navier-Stokes equations or Dirac equations.

ii) If things are as above, this suggests a deeper relationship between embedding theories and partial-differential equations. More specifically, embedding approaches suggest that modelling using partial-differential equations would only consider the regular part of dynamical behaviours. In the same time, these equations cannot surprise in any way the turbulent solutions. The existence of so-called *weak solutions* or *strong solutions* means the existence of a supplementary structure which exists beyond the regular solutions, and which can only be surprised by the principles of minimal non-differentiable action.

REFERENCES

- Cresson J., *Scale Calculus and the Schrödinger Equation*, Journal of Mathematical Physics, **44**, 11, 4907-4938 (2003).
- Cresson J., *Fractional Embedding of Differential Operators and Lagrangian Systems*, Journal of Mathematical Physics, **48**, 3 (2007).
- Cresson J., Darses S., *Stochastic Embedding of Dynamical Systems*, Journal of Mathematical Physics, **48**, 7, 072703 (2007).

TEORIA “EMBEDDING” PENTRU SISTEME COMPLEXE

(Rezumat)

În acest articol prezentăm o introducere în teoria “embedding”-ului, care este o metodă de descriere matematică a proceselor fizice foarte neregulate în sisteme complexe, cum ar fi turbulențele fluide sau acele procese care apar la nano-scală, folosind un operator de derivare extins.